A MINIATURIZED LOW POWER MILLIMETER WAVE RFID TAG FOR SPATIAL LOCALIZATION AND DETECTION

A Thesis
Presented to
The Academic Faculty

By

Ajibayo O. Adeyeye

In Partial Fulfillment
of the Requirements for the Degree
Master of Science in the
School of Electrical and Computer Engineering

Georgia Institute of Technology

August 2022

A MINIATURIZED LOW POWER MILLIMETER WAVE RFID TAG FOR SPATIAL LOCALIZATION AND DETECTION

Approved by:

Dr. Manos Tentzeris, Advisor
School of Electrical Engineering
Georgia Institute of Technology

Dr. Gregory Durgin
School of Electrical Engineering
Georgia Institute of Technology

Dr. Andrew Peterson
School of Electrical Engineering
Georgia Institute of Technology

Date Approved: June 13, 2022

TABLE OF CONTENTS

List of Figures vii

Summary ix

Chapter 1: Introduction and Background 1

Chapter 2: Core Technologies 6

2.1 Backscatter 6

2.2 FMCW RADAR 7

2.2.1 FMCW Signal Processing/Analysis 8

Chapter 3: Tag Design 14

3.0.1 RF-Front End 14

3.0.2 Baseband Circuitry 19

3.0.3 Energy Harvesting 19

3.0.4 Final Tag Design and Fabrication 22

Chapter 4: Parameter Extraction and Signal processing 25

4.1 Reader Architecture 25

4.2 Tag Identification and Detection 25

4.3 Ranging 26

4.3.1 Signal Processing Flow for Range Extraction 27

4.4 Angle of Arrival 40

Chapter 5: Conclusion 44

References 48

LIST OF FIGURES

1.1 RFID Application 1

1.2 ISM Frequency Bands 3

2.1 Backscatter [17] 6

2.2 Smith chart showing ideal antipodal reflection coefficients 7

2.3 FMCW Block Diagram 9

2.4 FMCW Signal Model 10

2.5 FMCW Angle of Arrival 13

3.1 System Block Diagram 15

3.2 Collocated Bi-Static Configuration 16

3.3 Cross polarized patch antenna design 17

3.4 CE3520K3 Switch [27] 18

3.5 Designed RF Front End 18

3.6 Baseband Circuit Block Diagram 20

3.7 Rectenna Block Diagram 21

3.8 Chip antenna [28] 22

3.9 ADS Schematic of Rectifier 23

3.10 Fabricated Chip Antenna based Energy Harvester 23

3.11 Fabricated Tag 24

4.1 Tag Identification [30] 28

4.2 Windowing Operation 29

4.3 Spectrum before and After Windowing 29

4.4 Spectral Binning in the Tag Response 30

4.5 Spline Interpolation 31

4.6 Spectrum Spline Interpolation Performance: (a) Measured vs. Real Distance Distribution (b) Error vs. Real Distance 32

4.7 Individual Spectrum due to multiple ramps 33

4.8 Averaged Spectrum 34

4.9 Spectrum averaging method performance: (a) Measured vs. Real Distance Distribution (b) Error vs. Real Distance 35

4.10 Modulation phase de-embedding 37

4.11 Phase based ranging: (a) Measured vs. Real Distance Distribution (b) Error vs. Real Distance 38

4.12 Phase based ranging (sub-mm): (a) Measured vs. Real Distance Distribution (b) Error vs. Real Distance 39

4.13 Angle of Arrival Calibration: (a) Before and after calibration at $0\,^{\circ}$ (b) Error vs. Before and after calibration at $-20\,^{\circ}$ 41

4.14 Angle of Arrival: (a) Measured vs. True Angle Distribution (b) Error vs. True Angle 43

SUMMARY

Research Objectives

The objective of this thesis is to show the applicability of millimeter wave RFID combined with radar principles for the accurate localization of an energy autonomous backscatter transponder. Specifically, the thesis focuses on these two main points:

1. The design and development of an energy autonomous millimeter wave RFID tag
2. Signal processing flow for the extraction of the relevant spatial angle and range information

Thesis Outline

The thesis is outlined as follows:

Chapter 1 introduces and provides some background and state of the art on the core technologies discussed in this work

Chapter 2 discusses the two core concepts important for the realization of the system proposed: backscatter modulation and FMCW radar

Chapter 3 presents the design of a miniaturized millimeter wave tag that is energy autonomous and ultra-low power

Chapter 4 details the specific signal processing schemes used to extract identification and localization information and presents obtained results and comparisons between some different methods

Chapter 5 provides concluding remarks to the work presented in the thesis and adds some notes on future applications

The work presented in 4.3.1 (Spectrum Spline Interpolation Method) was published in the 2019 European Microwave Week Proceedings and is reference [30] in this thesis

CHAPTER 1

INTRODUCTION AND BACKGROUND

Radio Frequency Identification (RFID) technology has become increasingly pervasive in modern technologies and applications over the last few decades. RFID has proved extremely useful for a multitude of wireless systems applications, owing to its relatively low costs of manufacturing and deployment in addition to its potential for energy autonomy (operation without batteries). A multitude of RFID based technologies have already been deployed in a wide variety of industries including but not limited to the logistics, healthcare, security and the retail industries [1, 2, 3, 4, 5, 6].

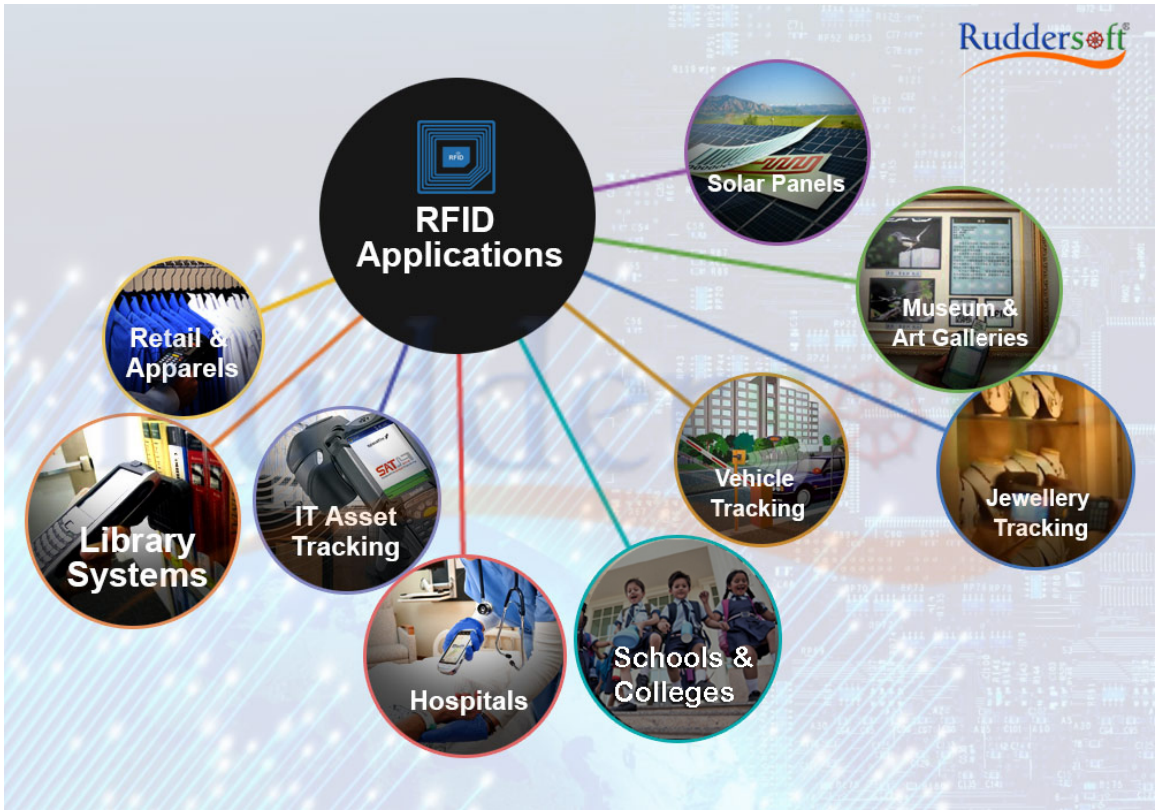

Figure 1.1: RFID Application

An RFID system typically consists of two main components namely the “reader” and

the “tag”. The reader’s primary function is to generate and transmit an interrogation signal at a set frequency and to subsequently process the returned signal from the tag which would usually contain some unique identifier from the tags in its vicinity. RFID tags can be grouped into three main categories namely: active, semi-passive and passive RFID tags. This categorization is done based on the manner in which the tags communicate and are powered. Active RFID tags have an on-board power source which it uses to power any additional electronics as well as generate its own RF signal for communication. Passive and semi-passive RFID tags make use of the interrogating signal received from the reader to communicate via backscatter modulation. The difference between these two however is that the fully passive RFID tags depend on energy harvested from the interrogation signal to power up while the semi-passive tags have an on-board power source similar to the active tags but much lower power is required since there is no RF signal generated locally. The major trade-offs between these three RFID tag architectures is in the read range, power consumed and invariably the cost of manufacturing and scalability of the tags depending on the required application.

A large amount of existing RFID technology applications is deployed in the Ultra High Frequency (300 MHz to 3 GHz) band. However, power limitations, limited available bandwidth and the multitude of devices operating in this frequency band has encouraged research and exploration into the use frequencies of operation in the millimeter wave regime. This creates a unique opportunity in conjunction with the advent of Fifth Generation (5G) wireless technology which seeks to connect a swarm of devices supporting high data rates whilst utilizing the readily available millimeter wave frequency bands. A system operating in the 24 GHz Industrial, Scientific and Medical (ISM) band fits the bill for compatibility with 5G wireless technologies and increased available bandwidth. In addition, the use of millimeter wave frequency bands enables the development of a very low form factor RFID tag which makes this system suitable for ubiquitous dense implementations in an array of short-range identification and localization implementations.

Center Frequency	Bandwidth	EIRP
915MHz	26 MHz	36 dBm
2.45 GHz	100 MHz	36 dBm
5.8 GHz	150 MHz	36 dBm
24 GHz	250 MHz	12 dBm
60 GHz	7 GHz	12 dBm

Figure 1.2: ISM Frequency Bands

A popular application of RFID technology and the primary focus of this work is its use as a means for the spatial localization and tracking of objects in a close range. It is important to note here that the system of localization described here differs from wireless local positioning systems in which a network of readers and transponders are used for localization and tracking along with trilateration or multi-angulation techniques. In the system being considered, the two quantities of interest that enable localization are the distance from the reader to the tag as well as the relative angle of the tag with respect to the reader [7, 8, 9].

The determination of the range and relative angle and consequently the location of an RFID tag in space is achieved via two main principles: round-trip time of flight (RTOF) and the received signal strength (RSS). The RTOF is the total time it takes for the interrogating signal to propagate towards the RFID transponder and back while the RSS is the amplitude of the interrogation signal received after round-trip propagation. With the RTOF method, the propagation time is easily mapped to a range simply by knowing the speed of propagation within the specific media (in free space, $c = 3 \times 10^8\,\mathrm{m/s}$). The RSS method takes advantage of the relatively linear variation in the loss of signal strength with distance in addition to the phase of the received signal which enables the distance to be obtained as a fraction of a wavelength [1].

The work outlined in this thesis investigates the applicability of millimeter wave semi-passive backscatter nodes for use in the spatial localization and tracking of objects at short

distances. A miniaturized semi-passive ultra-low power energy autonomous RFID tag operating in the 24 GHz ISM frequency band is developed. The spatial localization of the RFID tags is enabled by the use of a Frequency Modulated Continuous Wave (FMCW) Radar as the reader. The radar is used to resolve the modulated backscatter returned by the RFID tags when interrogated by a Continuous Wave from the reader. The spatial information (range, angle with respect to the reader antenna) is contained in the returned signal's peak frequency and phase. The returned data is processed digitally in order to extract the required information regarding the spatial location of the RFID tag. The selection of the 24GHz ISM band makes FMCW radar an attractive option for localization of backscatter transponders for a number of reasons:

1. Large available bandwidth (up to 250 MHz)
2. Operates with low power compared to other modules
3. Low cost commercially available chipsets in this frequency band
4. Small form factor with easily integrated customizable antenna arrays
5. A single radar can be used to localize and identify multiple backscatter transponders thus improving scalability

There have been various efforts reporting the use of FMCW radar-based detection with active backscatter modulating RFID tags for use in localization and detection. The work presented in [10] evaluates an active backscatter target operating at 34.45 GHz based on a switched injection-locked oscillator (SILO) concept localized using a conventional FMCW radar system. The SILO developed in [11] is used as a regenerative amplifier on the mobile tag. The SILO is used to overcome certain challenges with Radar detection such as the decay in received signal power by the inverse of the fourth power of the distance between the tag and radar. Since the signal emitted by the tag is spontaneous and not a modulated duplicate of the interrogation signal, the received signal power decays by the inverse of the

second power of the reader to tag distance. While the methods used in this effort yields desirable results in range accuracy (mean error of 7cm for ranges up to 11.5m), the SILO amplifier consumes up to 0.122 Watts [10]. In addition to the relatively high-power consumption, the overall tag architecture presents a large form factor which would make it less suitable for tracking and localization of objects in a dense deployment in indoor/outdoor environments. An active backscattering two-dimensional positioning system is proposed in [12] also using the SILO system. This system makes use of a Time-Series Post-processing technique in combination with the SILO principle on the active backscatter tag. The post-processing technique used in this effort is based on subspace decomposition as opposed to the more commonly implemented Fast Fourier Transform (FFT) approach to multi-target discrimination. A primary advantage of this method is that it is indifferent to aliased peaks of multiple targets in the frequency domain while in the FFT approach, the modulation frequency needs to be sufficiently staggered so that the peaks can be differentiated for target differentiation. The subspace decomposition technique also benefits from inherent noise reduction so there is also some gain in the signal-to-noise ratio (SNR). The localization system proposed here suffers similar limitations to that proposed in [10] such as increased power consumption on the tag, large target form factor as well as the requirement of a bulky/expensive reader. The work presented in [13] identifies a unique opportunity for ultra-long range, low power wireless sensing using a custom millimeter wave RFID tag. The tag is comprised of an antenna, minimalist backscatter modulation front end and an energy source.

CHAPTER 2

CORE TECHNOLOGIES

2.1 Backscatter

One of the most important concepts involved in the work done in this thesis is the use of backscatter modulation. Backscatter communication is a relatively mature piece of technology having first been proposed in the 1940s and described as "Communication by means of reflected power". It has subsequently seen use in an array of modern applications most notably in passive RFID within the ultra-high frequency (UHF) band. These applications commonly consist of a single transistor or switch and an antenna. These tags are able to be activated using only the RF power from an illuminating continuous wave signal and thus can be operated without any external source of energy. In modulated backscatter, a radio-frequency (RF) tag is illuminated by an interrogating signal and the tag reflects the impinging signal back towards the transmitter with a reflection coefficient that is varied as a function of the load presented to the terminals of the antenna [14, 15, 16].

Typically found is switching between an open circuit and a short circuit load which implements a binary phase shift keying (BPSK). However, more complex modulation schemes

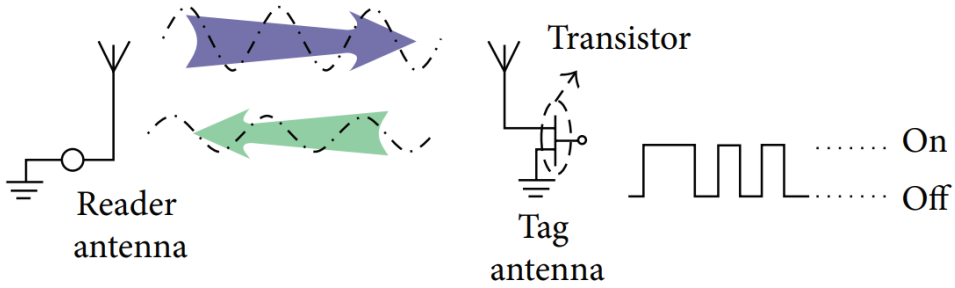

Figure 2.1: Backscatter [17]

have been found and suggested in literature for backscatter communications [14].

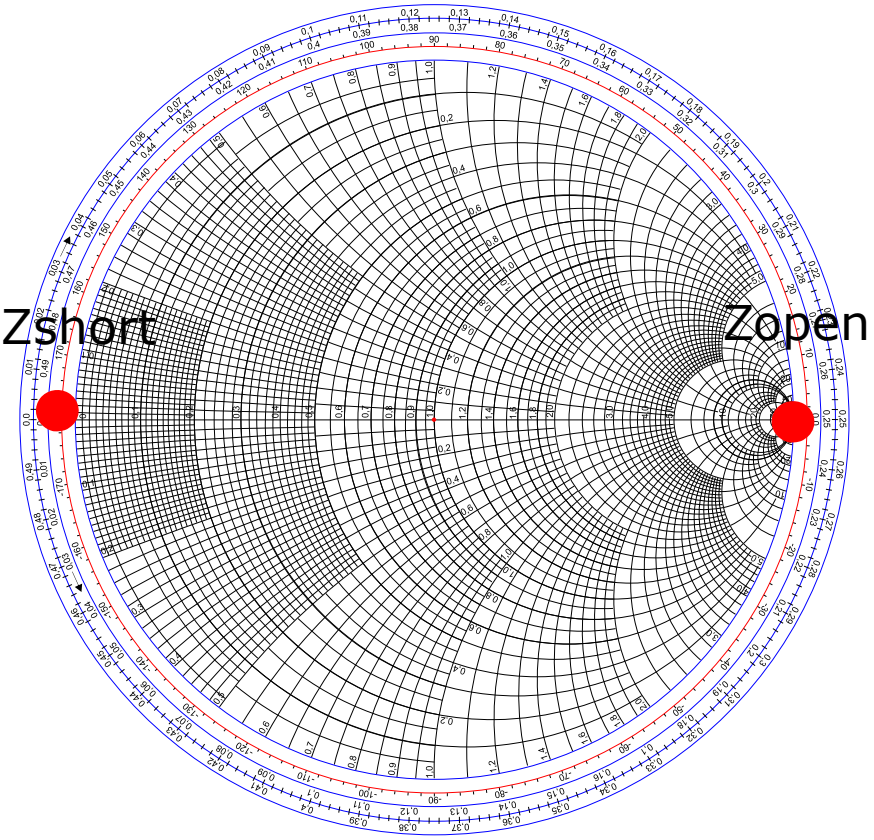

Figure 2.2: Smith chart showing ideal antipodal reflection coefficients

2.2 FMCW RADAR

The selection of the 24GHz frequency band for the designed system makes it imperative to choose a reader system and architecture that is compatible and is able to realize the ultimate goal of spatial localization and detection. There is an array of interesting research done at the intersection of RFID and radar systems largely due to the similarities in the challenges experienced in the operation of both with applications up to $60\,\mathrm{GHz}$ investigated [18, 19, 10, 20, 21]. FMCW is a fairly well known and widely deployed round-trip time of flight radar positioning system. FMCW radar comes with a few advantages over other radar schemes that make it a highly suitable choice for localization of backscatter targets such as:

1. Simplistic architecture makes it easy to manufacture at scale while maintaining low costs

2. Ability to simultaneously measure range, angle of arrival as well as velocity in a Multiple Input Multiple Output (MIMO) configuration

3. Highly accurate ranging at close distances and greater unambiguous range compared to CW

4. Low bandwidth baseband signal (typically $< 2\,\mathrm{MHz}$) means lower complexity in signal processing using a Fast Fourier Transform (FFT) algorithm

5. Relatively low/ power consumption

The theory of operation of FMCW radar at it's core is relatively simple, a continuous wave with a time varying frequency is sent by the transmitter and after reflection from a target at a given distance a delayed and attenuated copy of the transmitted signal is received. The auto-correlation of the transmitted and received signals is produced using a mixer which generates two signals: one with a phase that is the sum of the phases (sum signal) of the correlated signals and one with a phase equal to the difference of the phases(difference signal) [22]. The sum signal generally represents a high frequency component of the baseband signal and is filtered out using a low pass filter so that the difference signal having the required spatial information is passed on to the signal processing unit.

2.2.1 FMCW Signal Processing/Analysis

The important question at this juncture is how exactly the range and angular information is encoded in the baseband signal output. Phase is typically used for range finding in chip-less implementations where a sinusoid at a fixed frequency is used to excite a target and the returned signal is processed to extract the range. The returned signal takes the form described in equation 2.1 where A is the amplitude of the signal being a function of

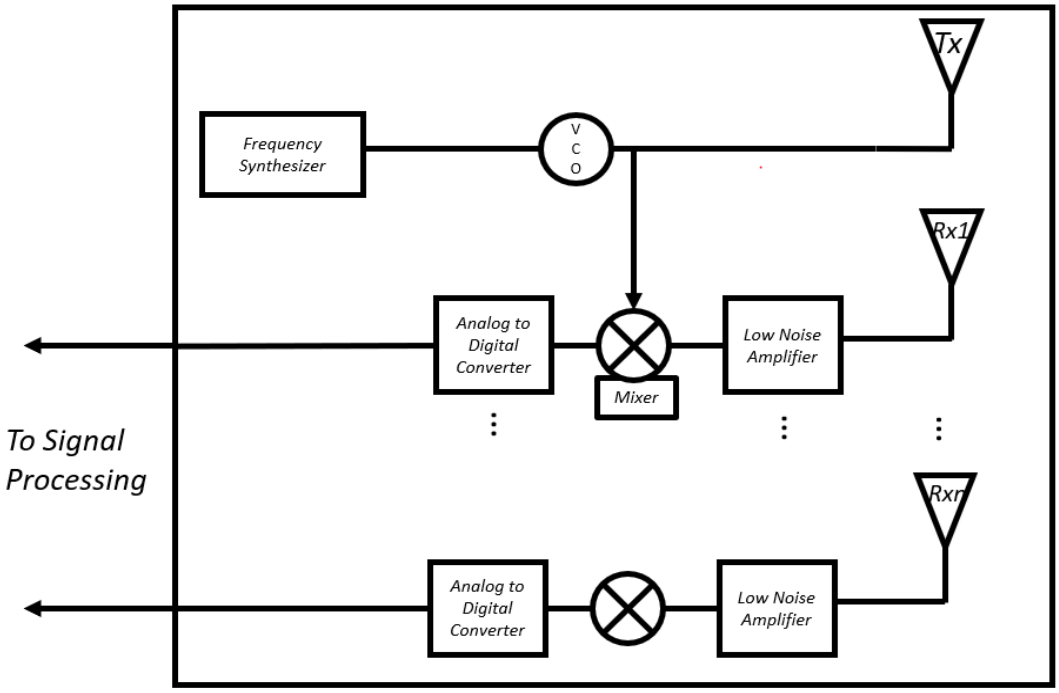

Figure 2.3: FMCW Block Diagram

frequency and position, f_0 is the frequency of the excitation signal, k is the wavenumber (or propagation constant$= 2\pi/\lambda$) where λ is the wavelength of the interrogating signal in the medium of propagation which is generally free space for wireless range finding applications and R is the distance between the reader and target. However, a major limitation in this method is the unambiguous range achieved in using the round-trip phase accumulation between the target and the reader to extract the distance between the two.

$$X = Acos(2\pi f_0 - 2kR) \tag{2.1}$$

In FMCW, the carrier (or center) frequency of the interrogating signal is varied continuously as a function of time. This function can be linearly varying (sawtooth, triangular etc.) or nonlinear (sinusoidal, exponential). This time dependence of phase in the FMCW method makes it a much more attractive option for range finding in this context. The work presented here considers only the case of a linear dependence of frequency and time that can be modeled by equation (2.2) where f_{min} is the lowest frequency in the band of interest,

B is the sweep bandwidth and T_r is the period of the frequency sweep.

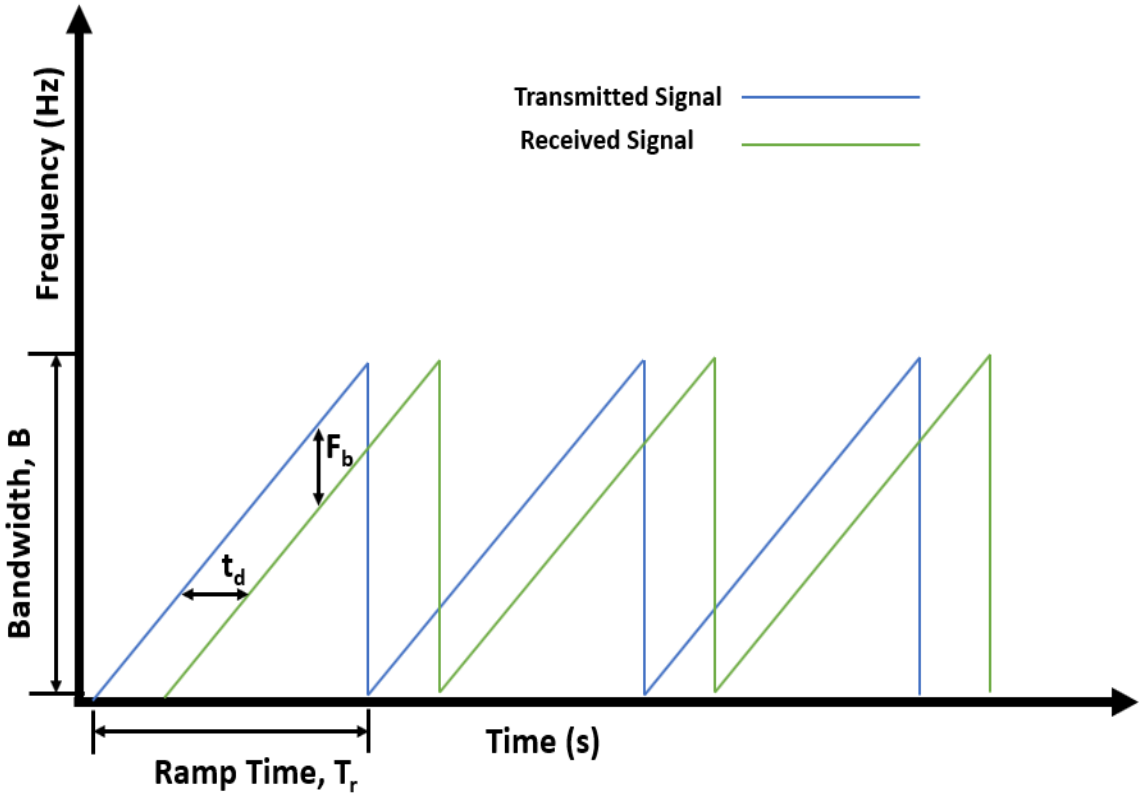

Figure 2.4: FMCW Signal Model

$$F(t) = f_{min} + \frac{B}{T_r}t \tag{2.2}$$

For simplicity in the subsequent derivations, we can denote the slope of the linear frequency sweep with $\alpha = B/T_r$ which represents the rate at which the full available bandwidth is swept. Integrating this time dependent frequency over time provides the instantaneous phase of the interrogating signal

$$\phi(t) = 2\pi \int_0^t F(t)\, dt \; = 2\pi(f_{min}t + \frac{\alpha t^2}{2}) + \phi_0 \tag{2.3}$$

The signal transmitted by an FMCW reader assuming a normalized amplitude can then

be written as 2.4

$$S_{tx} = cos(\phi(t)) = cos(2\pi(f_{min}t + \frac{\alpha t^2}{2}) + \phi_0) \tag{2.4}$$

Considering a backscattering target at a distance, R from the FMCW reader and modulating with a frequency, f_{mod}, random initial phase ϕ_{mod} and a normalized signal amplitude. The radar cross section of the target is represented in time by 2.5

$$S_{tag} = cos(2\pi f_{mod}t + \phi_{mod}) \tag{2.5}$$

The transmitted signal propagates towards the target, is reflected and then travels back towards the reader over a period of time, $t_d = \frac{2R}{c}$. The received signal at the reader is a copy of the transmitted signal delayed by time t_d and scaled by the modulating RCS of the scattering target of interest. The signal S_{rx} can be written as in equation 2.6 with the variable $k = \frac{2\pi}{\lambda}$ representing the wavenumber of propagation in the given medium.

$$\begin{aligned} S_{rx} &= S_{tag}(t - \frac{t_d}{2}) * S_{tx}(t - t_d) \\ &= cos(2\pi f_{mod}(t - \frac{t_d}{2}) + \phi_{mod}) * cos(2\pi(f_{min}(t - t_d) + \frac{\alpha(t - t_d)^2}{2}) + \phi_0 + 2kR) \end{aligned} \tag{2.6}$$

Upon reception, the received signal S_{rx} is brought to baseband by mixing with the transmitted signal S_{tx}. This results in the baseband signal S_b defined as in equation 2.7. The sum term in the cosine multiplication will result in a very high frequency output on the order of $2f_{min}$ which will be filtered out so for simplicity in expression, this term can be ignored. The difference term then contains the required de-chirped baseband signal that passes through the low-pas filter. The quantity $\alpha t_d = \frac{B}{T}\frac{2R}{c}$ is the beat frequency and contains the required ranging information for the target and is denoted by f_b. Upon

simplification, we see that we get two frequencies: $f_{mod} + f_b$ and $f_{mod} - f_b$.

$$
\begin{aligned}
S_b &= S_{rx} * S_{tx} \\
S_b &= S_{tag}(t - \frac{t_d}{2}) * S_{tx}(t - t_d) * S_{tx} \\
&= S_{tag}(t - \frac{t_d}{2}) * cos(2\pi(f_{min}(t - t_d) + \frac{\alpha(t - t_d)^2}{2}) + \phi_0 + 2kR) * cos(2\pi(f_{min}t + \frac{\alpha t^2}{2}) + \phi_0) \\
&= S_{tag}(t - \frac{t_d}{2}) * cos(2\pi(f_{min}(t_d) + \alpha t_d t - \frac{\alpha {t_d}^2}{2} - 2kR) \\
&= S_{tag}(t - \frac{t_d}{2}) * cos(2\pi(f_b t + (f_{min} - \frac{f_b}{2})t_d) - 2kR) \\
&= cos(2\pi f_{mod}(t - \frac{t_d}{2}) + \phi_{mod}) * cos(2\pi(f_b t + (f_{min} - \frac{f_b}{2})t_d) - 2kR) \\
&= \frac{1}{2}cos(2\pi((f_{mod} + f_b)t + (f_{min} - \frac{f_b + f_{mod}}{2})t_d) + \phi_{mod} + 2kR) + \\
&\frac{1}{2}cos(2\pi((f_{mod} - f_b)t - (f_{min} + \frac{f_{mod} - f_b}{2})t_d) + \phi_{mod} - 2kR)
\end{aligned}
\tag{2.7}
$$

An FFT can be applied to the sampled baseband signal and the difference between the two frequency peaks is taken which results in $2f_b$. The range, R of the target is then given by $R = \frac{f_b}{2\alpha}$c. This analysis is valid for extracting the range of a static backscattering target. A more intensive signal analysis is required for moving targets taking into account doppler effects. In summary, the time dependence of the center frequency results in a similar time dependence of the resultant phase of the baseband signal after down conversion which is a frequency in and of itself. Consequently, using the FMCW process it is possible to map the phase of the interrogating and received signals to a frequency and subsequently extract the range of the backscattering target.

Using the FMCW process, it is also possible to determine the angular position of a backscattering target relative to an interrogator. This can be achieved by making a simple modification to the receiver architecture. It is necessary to add additional receiving channels so that well known phase interferometry techniques can be used to extract angular information. For a target at a given range interrogated using an FMCW radar, there is an

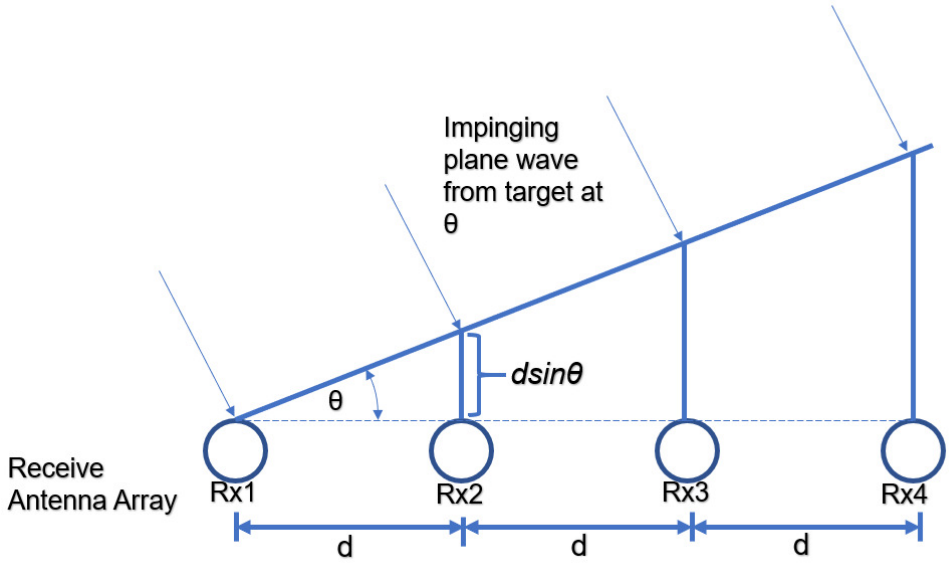

Figure 2.5: FMCW Angle of Arrival

associated beat frequency as described by equation 2.7. This beat frequency has an associated phase such that if there exists a given number of antennas separated by some fixed distance, each of them would experience a different phase shift that is dependent on the relative angle of the target this comes from the well known principle of interferometry. If there exist a set of equally spaced receiving antennas and a target in the far-field such that the electromagnetic wave scattered back can be assumed to be plane-waves of constant phase then we can see as illustrated in figure 2.5, the signal will arrive at each successive antenna after propagating an additional distance given by $dsin(\theta)$ relative to the previous antenna where d is the spacing between antennas and θ is the angle of arrival of the signal relative to the plane of the receiving antennas. The antenna spacing is commonly chosen to be $\frac{\lambda}{2}$ to obey the Nyquist-Shannon sampling theorem applied to this spatial sampling context as frequency in the conventional sense is paralleled with the wavenumber k. The additional distance travelled corresponds to a additional phase propagation of $\frac{2\pi dsin(\theta)}{\lambda}$. This is reflected in the phase of the beat signal as in equation 2.7. The FFT algorithm can then be applied across the sampled data from each of the receiving antennas to reveal spectral peaks that correspond to the required angle of arrival.

CHAPTER 3

TAG DESIGN

The use of millimeter wave frequency bands (the 24GHz ISM band in this case) permits the design and development of smaller and lower profile RFID tags compared to the state of the art and current widespread deployment of conventional implementations particularly in the UHF frequency range. The proposed RFID tag is comprised of two primary subsections: the RF front end and the supporting baseband circuitry. The RF front end includes a radiating element operating in the chosen frequency band as well as a single RF transistor which enables backscatter modulation based on load switching. The supporting baseband circuitry includes a low power oscillator used to generate a low frequency signal that drives the transistor, a low power consumption voltage regulator to ensure stability of the modulating signal, an energy storage element (e.g. a super-capacitor) and an energy source that could vary based on the selected application however in this work a chip antenna based energy harvester is investigated for application.

3.0.1 RF-Front End

Antenna

An integral part of the RF front end is the radiating element chosen. The antenna plays an important part in the ultimate performance of the designed RFID tag. One reason for this is explored in a quick evaluation of the link budget of the received modulated backscatter link. The particular link considered in this work is the bi-static, collocated backscatter link where the interrogating transmit and receive antennas are located in the same area separated by some fixed distance (a few wavelengths)[23].

The complete linear scale link budget for the received modulated backscatter power, P_R is given by equation 3.1. Where P_T is the power transmitted by the reader in watts, G_T is

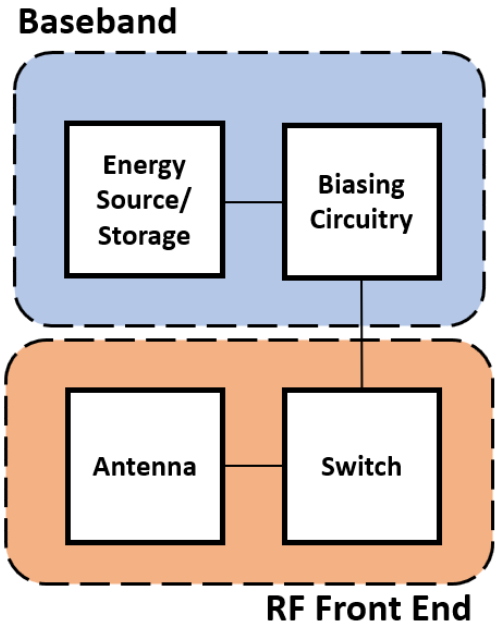

Figure 3.1: System Block Diagram

the gain of the reader transmit antenna, G_R is the gain of the reader receive antenna, G_t is the gain of the tag, λ is the wavelength in the medium of transmission,χ is the polarization mismatch, M is the modulation factor, r is the distance between the reader and the tag, Θ is the gain penalty due to the placement of the tag on an object B is the path-blockage loss and F_α is the fade margin,

$$P_R = \frac{P_T G_T G_R {G_t}^2 \lambda^4 \chi^2 M}{(4\pi r)^4 \Theta^2 B^2 F_\alpha} \tag{3.1}$$

From the link budget equation defined, we see that in linear scale the gain of the tag antenna is squared so the directivity provided by the chosen radiating element effectively counts in both the forward link where it integrates the incident energy and in the return link where the modulated signal is re-radiated. Thus, it is important that the antenna selected is well matched and high enough gain to ensure an acceptable link budget defined by the requirements of the system while maintaining a fairly broad beam-width so that interrogation is possible from a variety of different angles.

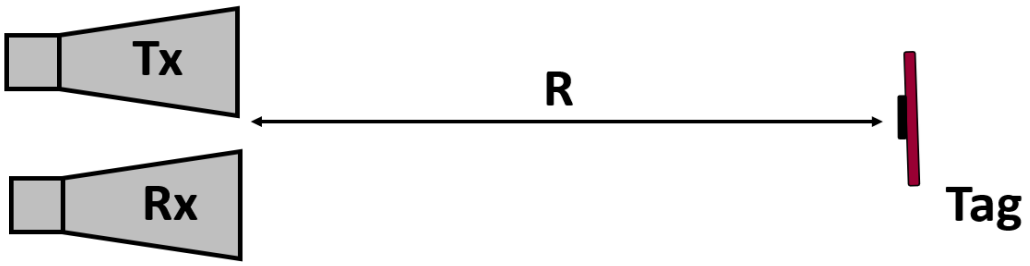

Figure 3.2: Collocated Bi-Static Configuration

The design of the radiating portion of the RF front end can be further optimized to improve limitations commonly found in backscatter and radar systems. One such limitation arises from mutual self-interference between the transmitting and receiving channels which is particularly problematic given the collocated backscatter link. The interrogating signal sent from the transmitting antenna is able to couple back into the nearby receiving antenna effectively degrading the signal to noise ratio of the link. Various methods have been proposed to mitigate the issue of self-interference in radar systems [24] one of them being the employment of a dislocated backscatter link such that the receiving antenna is located some distance away from the transmitter. This method is effective however it comes at the cost of a much larger system overall and becomes unsuitable for implementations where a single low-cost reader is preferred. In this effort, the antenna element is designed such that the interrogating continuous wave signal is re-radiated after modulation in an orthogonal polarization to that which was received. When interrogated with a similarly cross polarized transmitting and receiving antennas at the reader there is improved self-interference rejection at the reader on the order of 20+ dB [25, 26]. This allows improved sensitivity while maintaining a low-cost low form factor reader.

Given the requirements for a high-gain, low profile, surface conformal tag that can be cross-polarized, a simple patch antenna proves to be a very good choice. The ground backed design of the patch antenna makes it particularly attractive owing to the fact that

it can then be deployed on a variety of different surfaces without significantly affecting its performance. The antenna is designed and simulated in CST Microwave Studio. The patch antenna is made square in order to ensure matched impedance in both polarizations so that a transformer is not required and the connection between both polarizations can be made using a transmission line made to be a multiple of a half wavelength. The antenna is designed to operate at a center frequency of 24.125 GHz so it can capably cover the allotted 250MHz of ISM allocated bandwidth that ranges from 24-24.25GHz.

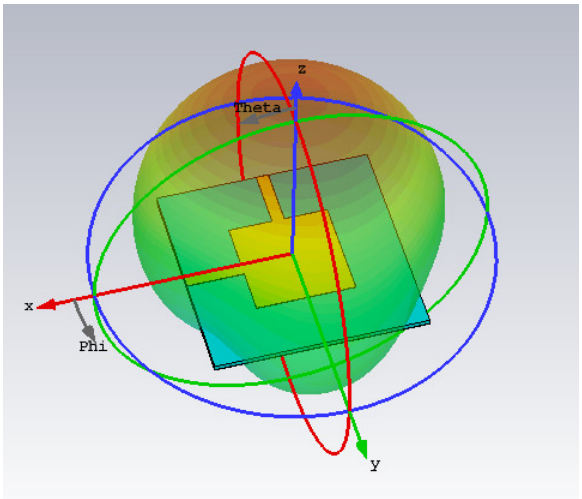

Figure 3.3: Cross polarized patch antenna design

Switch

The second part of the RF front end structure is the switching architecture that enables load modulation for the backscatter communication. The modulating portion of the front end is made up of a single low noise FET (CE3520K3) from California Eastern Laboratories and a set of radial stubs for isolation and load representation. The CE3520K3 is chosen for a variety of desirable performance features, it features a very low input gate capacitance and gate to source leak current such that the combined power consumption of the transistor due to the switching characteristics and current leakage is low thus driving down the overall power consumption of the front end.

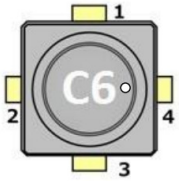

Pin No.	Pin Name
1	Source
2	Drain
3	Source
4	Gate

Figure 3.4: CE3520K3 Switch [27]

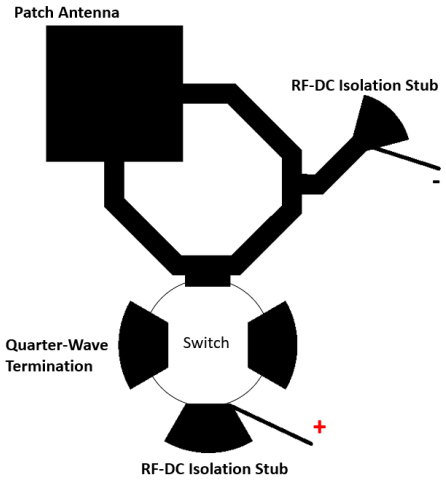

Figure 3.5: Designed RF Front End

The FET in use is biased across the gate and drain pins as opposed to conventional gate-source biasing due to the fact that the drain and source pins are internally connected in the zero-bias condition such that when a bias voltage is applied to the gate pin the switch is open. The pair of source pins are terminated with quarter wavelength stubs representing a short circuit so that an incident wave will see a short circuit in the zero bias condition and will be reflected with a reflection coefficient, $\Gamma = -1$. In the biased condition, the stub is designed so that the incident wave sees an open circuit and is reflected with $\Gamma = +1$. Additional stubs are included at the points of DC bias to enable RF-DC isolation for optimal performance.

The switch is designed, and the layout is done using Keysight Advanced Design System. The design is done so that there is at least a difference of about 6dB in the two switched states at the desired operation frequency as demonstrated in [13].

3.0.2 Baseband Circuitry

The baseband circuitry employed comprises of an energy source, an ultra-low power consumption voltage regulator and a low power oscillator. The voltage regulator is selected to maintain a constant bias voltage across the input of the transistor in order to ensure the most consistent possible performance over time while maintaining power consumption as low as possible. The oscillator is a critical component in the biasing baseband circuitry of the designed backscattering RFID tag. The CSS555 timer is chosen for its low power consumption and relatively high degree of stability. The stability of the oscillator plays a vital role in the performance of the RFID tag because a jittery device would introduce a large amount of unwanted phase noise. The modulation frequency generated by the oscillator is determined by the R-C impedance of a fixed internal capacitance and a selected resistance value. This allows a great deal of flexibility and opens up many avenues for application possibilities with this simplistic and modular tag architecture. A supercapacitor is chosen as the energy storage element for the tag over a traditional coin cell battery for a variety of reasons. The supercapacitor is able to charge up to the target voltage much quicker than a battery in addition to having a longer lifespan in terms of the number of charge and discharge cycles that the device is able to undergo. In addition, the supercapacitor does not necessarily need an accompanying power management circuit to control its charging up. It can be charged up with a direct applied voltage as long as the supplied current is of an order low enough not to damage the device.

3.0.3 Energy Harvesting

While it is possible to make use of a pre-charged supercapacitor or battery for the purposes of evaluating the concept presented in this work, in order to present a more fully functional system an approach to ensure full energy autonomy of the developed tags is explored. The chosen method to supply energy to the RFID tag wirelessly is though RF energy harvesting. A rectenna is designed and implemented at 915 MHz to supply a charging voltage

to the supercapacitor to ensure continuous energy autonomous operation for tracking and localization capabilities. The area of RF energy harvesting is a well-researched field that focuses on energy conversion from ambient electromagnetic energy to usable DC voltage. This energy conversion is made possible through the use of a rectenna which is made up of an antenna, matching network, and some active device used for rectification which is usually selected to be a diode.

The first component in the rectenna system is the antenna which is chosen around some fixed constraints and requirements of the system. One of the main requirements of the RFID tag is that it maintains a relatively low form factor so that it fits with the desired application for short range localization in internet of things (IoT) applications. Fitting with this requirement, it is important for the antenna used in the energy harvesting circuitry to be small and low profile. In addition to the requirement for having a low form factor, the energy harvesting system must be able to supply the requisite voltage to charge up the supercapacitor and ensure stable continuous operation of the backscattering system. The voltage output of the rectenna is related directly to the radiated power available at the terminals of the antenna of the energy harvester. This available power is easily derived from the well known Friis' transmission equation 3.2 which provides a fundamental limit on the power available as a function of distance, equivalent isotropic radiated power (EIRP), frequency and antenna gain. Where P_{TX} is the power from the transmitter, D_{TX} and D_{RX} are

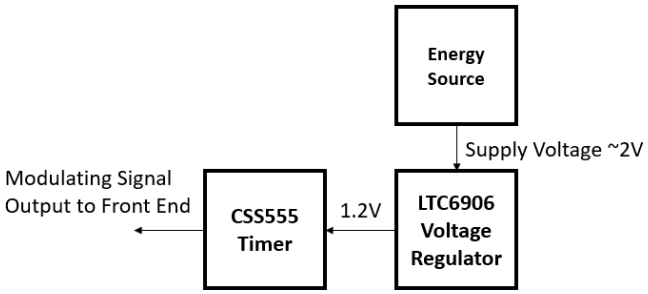

Figure 3.6: Baseband Circuit Block Diagram

the directivities of the transmitter and receiver respectively, λ is the free space wavelength and d is the distance between the RF source and the rectenna.

$$P_{av} = P_{TX} D_{TX} D_{RX} (\frac{\lambda}{4\pi d})^2 \tag{3.2}$$

The above equation shows quite simply that the efficacy of the antenna in integrating radiated power is critical to the performance of the energy harvesting system. This equation shows that a shorter wavelength (higher frequency) corresponds to a smaller effective antenna area and thus an antenna would be unable to integrate the radiated energy from the source as effectively as at a longer wavelength with the same physical area. This is an important note because for the same EIRP (max is 4W or 36 dBm) at the chosen 915 MHz band and a potential alternative e.g. 2.4 GHz, with the same physical antenna aperture, energy can be harvested more efficiently at the lower frequency. A chip antenna is chosen (ACAG1204-915-T from Abracon LLC.) as the radiating element for this rectenna to keep in line with the requirements for a low form factor module. Chip antennas are a class of dielectric resonator antennas made up of a parallel plate with a high permittivity dielectric in between. These antennas are generally specified with a lumped matching network and fixed ground plane size for optimal gain and radiation performance but for the purposes of this application the available ground plane size is fixed such that it is smaller than what is specified in the datasheet which deteriorates the antenna gain but for the proposed close range charging this is acceptable.

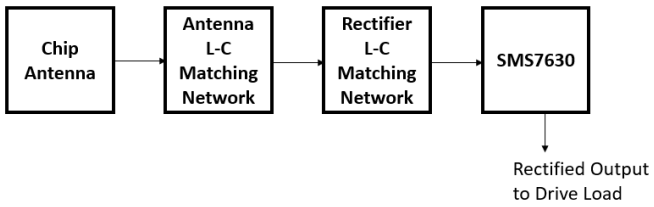

Figure 3.7: Rectenna Block Diagram

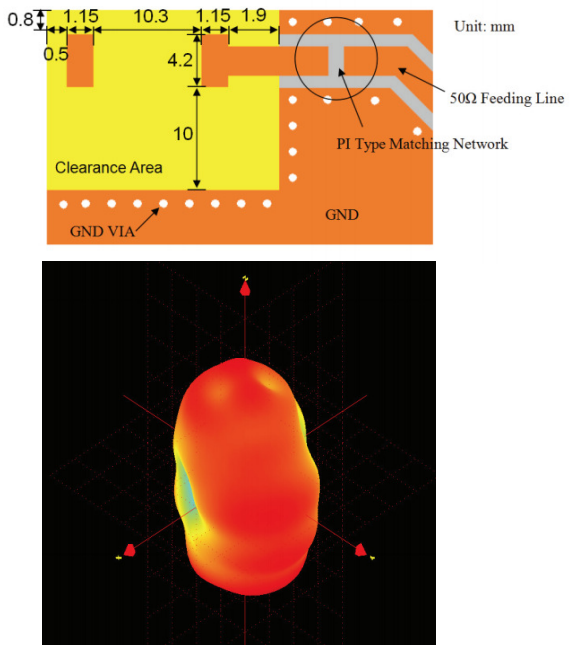

Figure 3.8: Chip antenna [28]

The second part of the rectenna system is the RF rectifying circuitry, which is made up of a matching network, a single Schottky diode in a series configuration. The diode chosen is the SMS7630 from Skyworks Solutions. The diode is chosen for its very low turn on voltage (approximately 0.17V). The rectifier is designed so that it is able to deliver the required voltage to charge the supercapacitor while in the far-field of the source. The matching network between the antenna and the diode is done using lumped components in an L-section matching configuration using a shunt inductor and a series capacitor so that the series component blocks DC into the load and permits the RF signal. The rectifier matching network is optimized in Keysight's Advanced Design System (ADS) to ensure diode activation at the lowest possible input power.

3.0.4 Final Tag Design and Fabrication

The tags used for measurement and analysis in this work are fabricated via an inkjet masking procedure and using a laser etching tool. Both of these methods prove to be rapid means for prototyping these small devices. The inkjet masking procedure consists of the

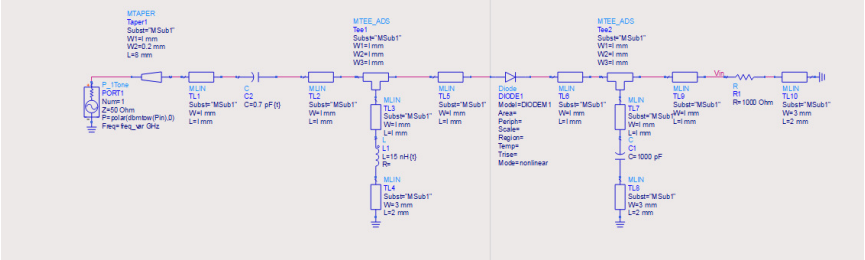

Figure 3.9: ADS Schematic of Rectifier

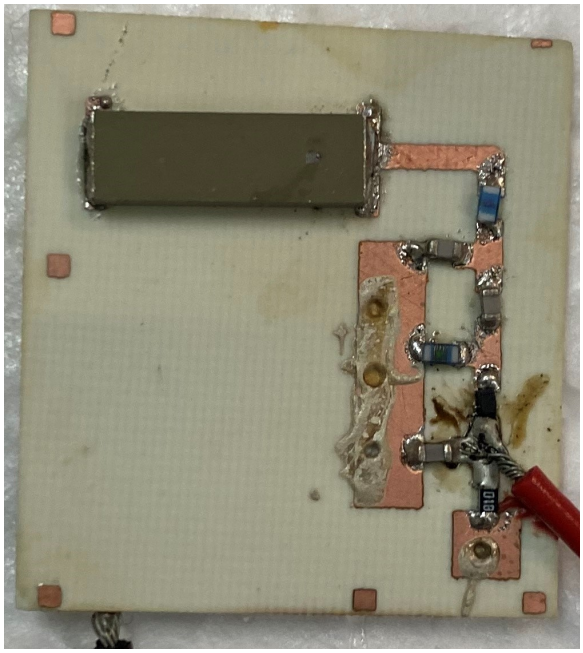

Figure 3.10: Fabricated Chip Antenna based Energy Harvester

inkjet printing of Microchem SU8 onto the copper clad surface of the chosen substrate. The SU8 acts like a positive photoresist where the parts of the copper covered by the SU8 remains insoluble and the rest of the exposed copper is etched away using a Iron Chloride solution as solvent.

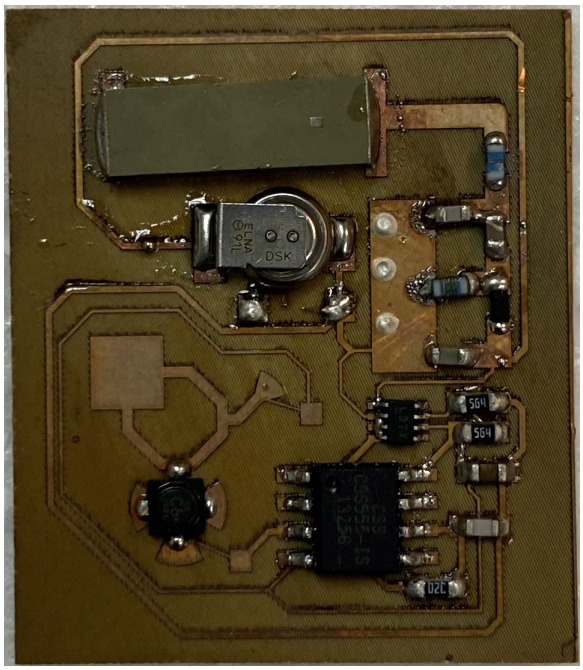

Figure 3.11: Fabricated Tag

CHAPTER 4
PARAMETER EXTRACTION AND SIGNAL PROCESSING

4.1 Reader Architecture

The reader used in this thesis is based on the low cost readily available 24 GHz chipsets from Analog Devices Inc. The fully integrated FMCW transceiver system is made up of the ADF5901, ADF4159 and ADF 5904 which are the transmitter, phase locked loop (PLL) and receiver, respectively. A convenient solution that integrates these three building block devices exists in the commercially available EVRADARMMIC2 development board made specifically for the evaluation of those chipsets in an FMCW context. The demodulated baseband signals from the four channels of the receiver are sampled on a Tektronix DPO 7454 oscilloscope. This sampled digital data is then saved on a mass storage device and imported into numerical analysis software for additional post-processing. A notable component of this reader architecture is the accompanying custom made cross polarized antenna module which is fabricated on a Rogers RO4003 substrate having thickness of about 350um. The antenna module is made up of four independent linear arrays in the receiving channel spaced by a half wavelength to ensure appropriate spatial sampling as well as two transmitting antennas operating in the orthogonal polarization. This custom antenna module enables very high resistance to self-interference caused by energy leakage between the collocated transmitter and receiver.

4.2 Tag Identification and Detection

The baseband signals are sampled by the oscilloscope at some fixed sampling rate which is dependent on a combination of the required unambiguous range and the modulation frequency of the RFID tag. To detect the presence of the RFID tag, a simple Fast Fourier

Transform (FFT) operation is applied. This reveals the frequency content of the sampled baseband signal and afterwards a peak search algorithm is run to locate pairs of spectral peaks that are precisely centered around the modulating frequencies of the tags of interest. The implication of this is that the modulating frequency of a tag in the field of view of the reader can be determined with no a-priori knowledge of the tag's characteristics with the only stipulation being that the antenna of the tag is properly tuned to that of the reader. It is known and was described in chapter 2 that for round trip time of flight based radar systems such as the FMCW, the distance of the target relative to that of the reader is directly proportional to the generated beat frequency which is a result of the mixing of the time-delayed and reflected chirp signal at the reader. When the delayed version of the interrogating signal is received on the RX channels, it is mixed with the signal that was sent in order to obtain a constant beat frequency which is representative of the total distance travelled by the signal. It is in the result of this process that one of the main advantages of using a backscattering system in combination with radar shows up. Although a cross-polarized interrogation scheme is employed, there is still a degree of self-interference between the transmit and receive channels such that the interfering signals show up as clutter around DC. The signal of interest is modulated away from the passive clutter and self-interference around DC which then allows for a much higher signal to noise ratio and increased sensitivity in detection.

4.3 Ranging

FMCW radar has been thoroughly investigated and presented in literature as particularly robust in determining the distance of a target with a sensitivity and accuracy relative to the system's parameters such as bandwidth, SNR and operating frequency. The specific limiting factor for important parameters such as range resolution and the accuracy of the distance measurement of the target has been found to be heavily dependent on the bandwidth over which the available signal information is integrated. Fundamentally the resolution limit is given by equation 4.1 where c is the speed of light in the medium and B is the available

bandwidth.

$$\delta_r = \frac{c}{2B} \tag{4.1}$$

The expression relating the accuracy and bandwidth is a bit more intricate and is shown via the Cramer-Rao bound for an unbiased frequency estimate and is defined for an FMCW radar in [29] and presented in equation 4.2 where r is the target range, v is the group velocity, N is the number of samples, B is the available bandwidth and η is the SNR.

$$var[r] = \frac{3v^2}{(2\pi)^2 \eta N B^2} \tag{4.2}$$

The bound shows a strong dependence on bandwidth and signal to noise ratio albeit a stronger relationship with the available bandwidth. Thus it can be inferred that increasing the available SNR or bandwidth invariably increases the achievable accuracy. However, given that the available bandwidth is limited by government regulations methods to improve ranging accuracy must be implemented in the subsequent signal processing. A backscattering target such as the one presented here presents a prominent advantage over conventional passive targets interrogated with an FMCW radar and that is reflected in the increased SNR for a given range.

4.3.1 Signal Processing Flow for Range Extraction

The baseband signal sampled on the oscilloscope is arrayed and imported into MATLAB for post-processing to extract the required information. The steps used revolve around the FFT operation used to reveal the frequency content of the given signal. The simple FFT operation is performed on the signal to reveal a spectrum as shown in figure 4.1. In this spectrum, the benefits of the amalgamation of FMCW and modulated backscatter is evident as it is shown that the tag response is able to be resolved further away in frequency from the static clutter and self-interference around $0\,\mathrm{Hz}$. The tag in this case is identified to be

modulating at approximately $40.4\,\mathrm{kHz}$.

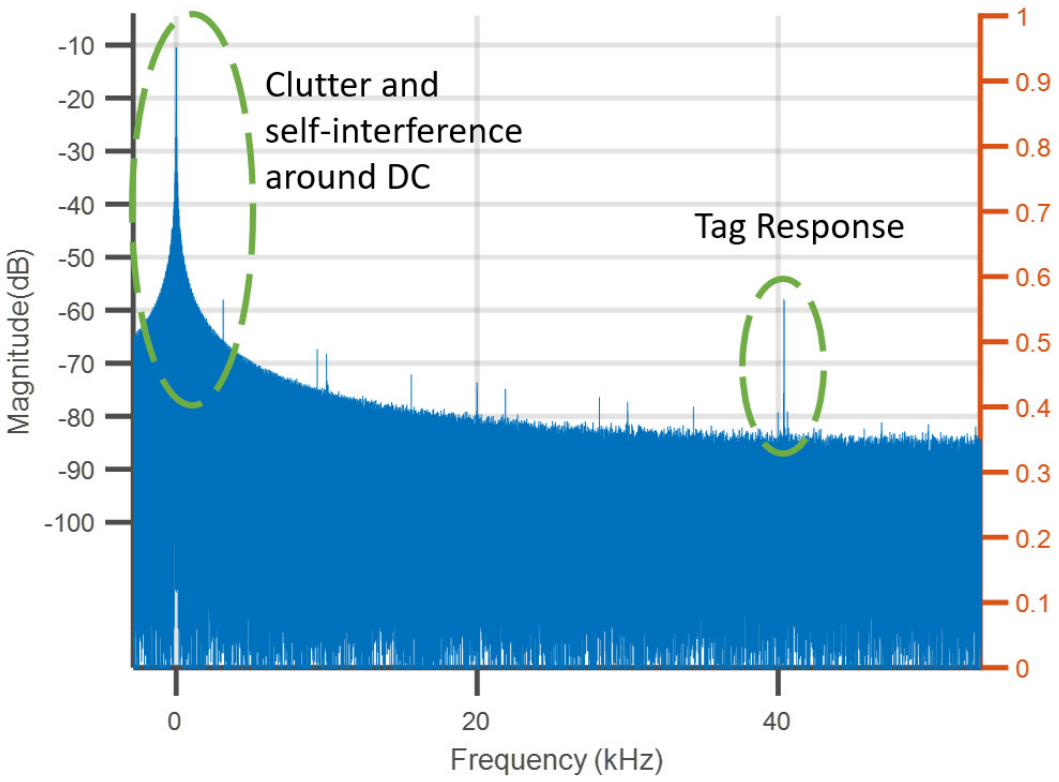

Figure 4.1: Tag Identification [30]

Prior to applying the chosen signal processing schemes to the arrayed signal, a short pre-processing step is required to improve the ultimate quality of the signal spectrum. A time-domain window is applied to the sampled baseband signal, this is done to mainly address the issue of discontinuity in the time domain in successive ramps and allows easy coherent integration of multiple ramps without much concern for resultant spectral leakage that inevitably occurs as a result of the random jumps in phase. This process is illustrated in 4.2 and the effect on the coherently integrated spectrum is shown in 4.3 where it is seen that the spectral leakage resulting from the discontinuities in successive ramps is eliminated around the desired tag information.

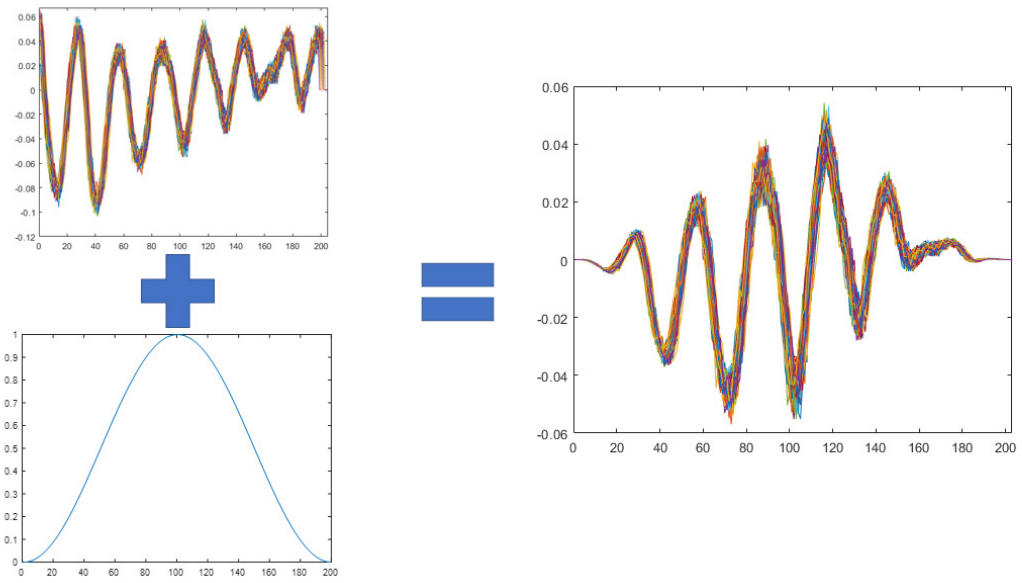

Figure 4.2: Windowing Operation

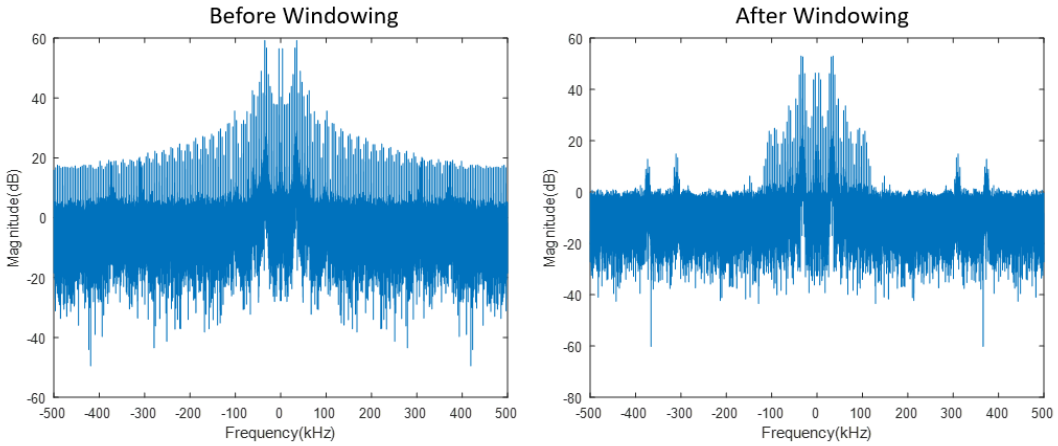

Figure 4.3: Spectrum before and After Windowing

Following the pre-processing step, the signal can then be analyzed via the FFT to extract the required range information. The following sub-sections describe two methods for extracting the range and presents the achieved accuracy in different configurations. A method applying the phase of the received signal to track the position of a tag finely over multiple millimeters and sub-millimeters is also described and presented.

Spectrum Spline Interpolation Method

In this process, the FFT is applied across all of the ramps coherently and as a result of the periodic discontinuities that result from the saw-tooth modulation, the frequency information of the tag is spread into frequency bins spaced evenly by the frequency of the applied FMCW signal given by $\frac{1}{T_{ramp}}$. Figure 4.4 shows the frequency response of the baseband signal zoomed in to the section containing information regarding the tag of interest showing the spectral binning effect. This effect limits the achievable accuracy of the proposed system so an additional step is required to reliably extract the range information. Here, a spline interpolation is applied to the evenly spaced samples as shown in figure 4.5 whereby the samples containing the frequency information of the tag are selected and a spline is used to interpolate between these samples over a fine scaled x-axis such that a more defined frequency peak can be revealed and the range of the desired target ultimately obtained.

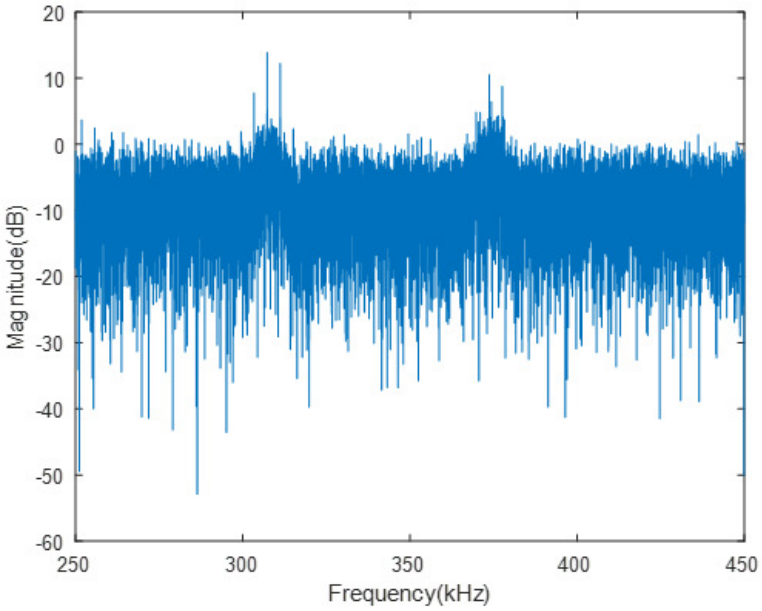

Figure 4.4: Spectral Binning in the Tag Response

The performance of this method of range extraction is verified experimentally by displacing the tag in front of the reader. The tag is fixed at an initial reference position and the moved in steps of $1, 2, 5, 10$ and $15\,\mathrm{cm}$. It should be noted that for the purposes of this ex-

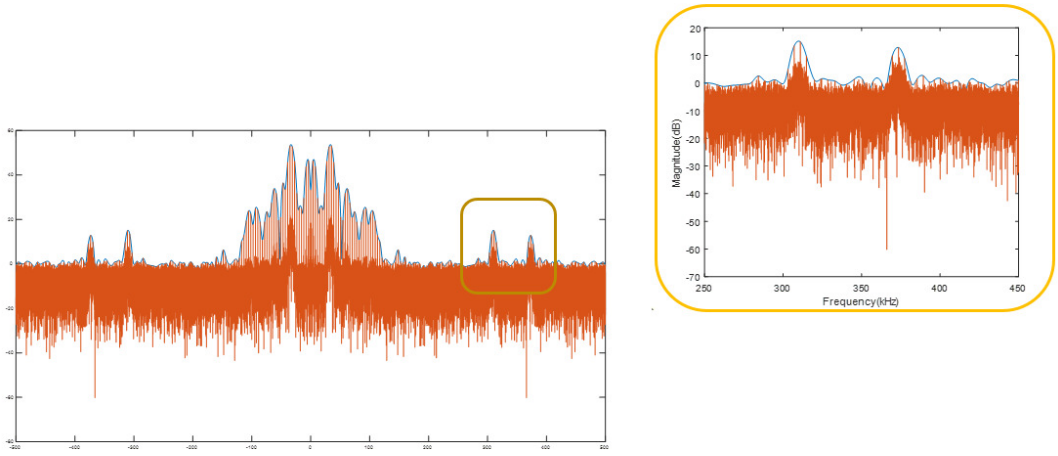

Figure 4.5: Spline Interpolation

periment the absolute distant between the reader and the tag is not evaluated, the sensitivity of the tag and reader system to displacement of the tag is used to evaluate the performance of the system. A total of ten measurements are taken at each point. The spline interpolation method is then applied on the sampled signals and the range is extracted from the difference between the two frequency components generated as described in chapter 2. Figure 4.6a shows the distribution of the measurements taken as the measured distance plotted against the real distance. Figure 4.6b shows the average error at each measurement point. The plot shows that using this method, the system is able to identify changes in distance to about $1.4\,\mathrm{cm}$ in the worst case.

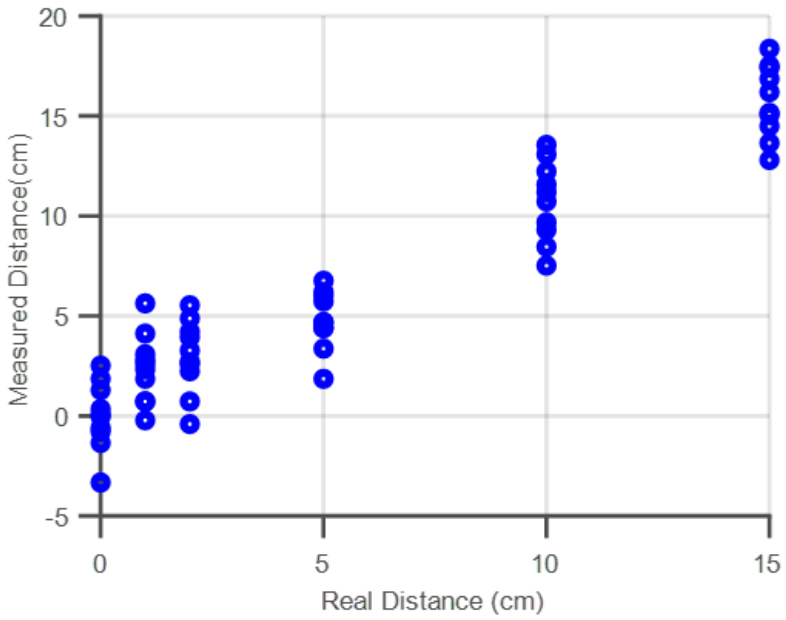

(a)

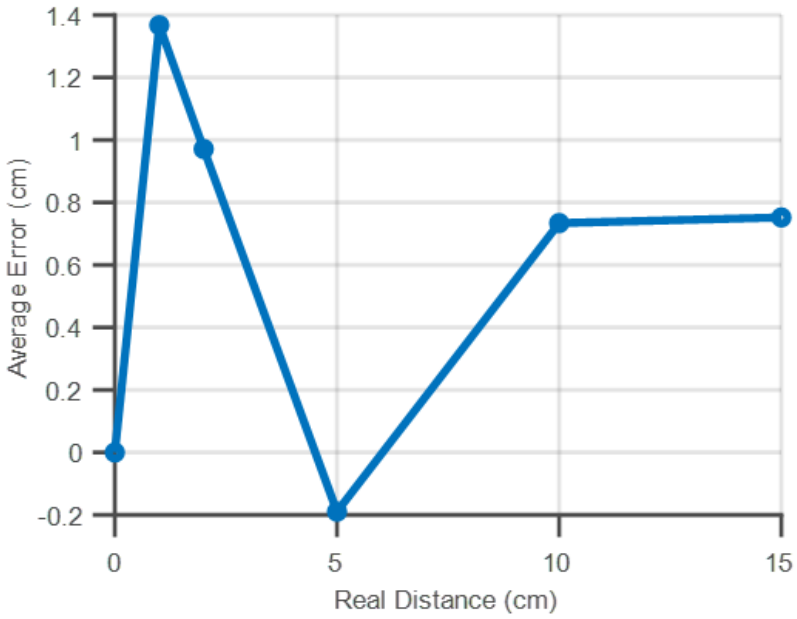

(b)

Figure 4.6: Spectrum Spline Interpolation Performance: (a) Measured vs. Real Distance Distribution (b) Error vs. Real Distance

Spectrum Averaging Method

In this method, instead of coherently integrating the baseband signals received from each ramp as in the previous case, here the baseband signal due to each ramp is processed independently and the resultant magnitude spectrum due to each ramp is averaged to produce a spectrum with a higher signal to noise ratio. The idea here is to take the response due to each ramp as a single observation then we have a number of total observations equal to the number of ramps processed then the noise can be averaged out over these many observations. It is important to note here that it is the magnitude of the spectrum being averaged and not the complex spectrum as the latter procedure would result in the signal of interest being averaged into the noise due the dynamic nature of the phase of the modulating target. Figures 4.7 and 4.8 show the individual spectrum from each ramp and the averaged spectrum respectively. It is clearly seen that the target of interest in 4.8 is resolved with much higher fidelity.

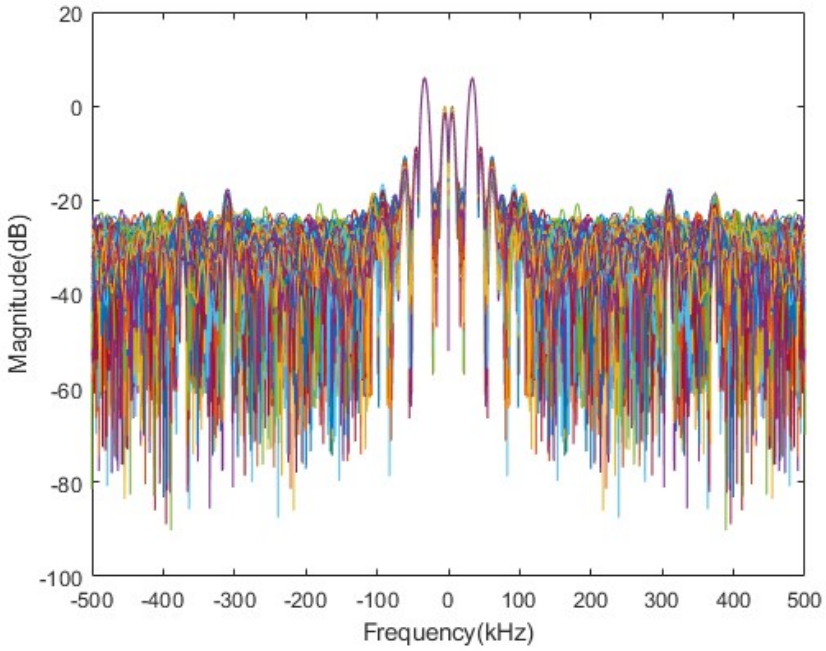

Figure 4.7: Individual Spectrum due to multiple ramps

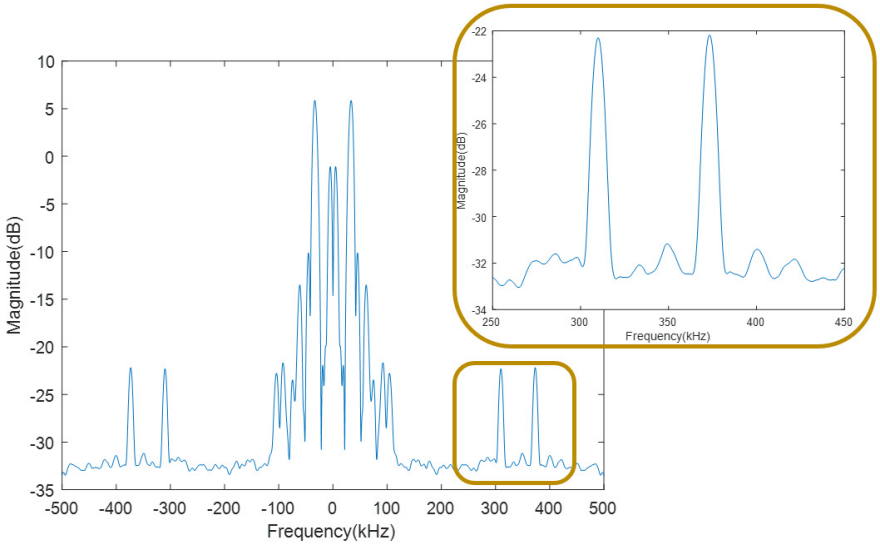

Figure 4.8: Averaged Spectrum

Like with the previous method, the performance of this signal processing step is verified experimentally by taking a tag at a given reference position and displacing it through a series of steps. The results of this are summarized in figures 4.9a and 4.9b. It is seen that in the employment of this method, the error in the distance measurement is kept below $0.25\,\mathrm{cm}$ more than 5x better than the error achieved using the previous method. In this method however, a large N-point FFT must be taken across each of the ramps amounting to N_{ramp} FFT operations of this size which may become computationally intensive thus depending on the application, either of the two developed range extraction methods could be employed with high accuracy ranging achieved.

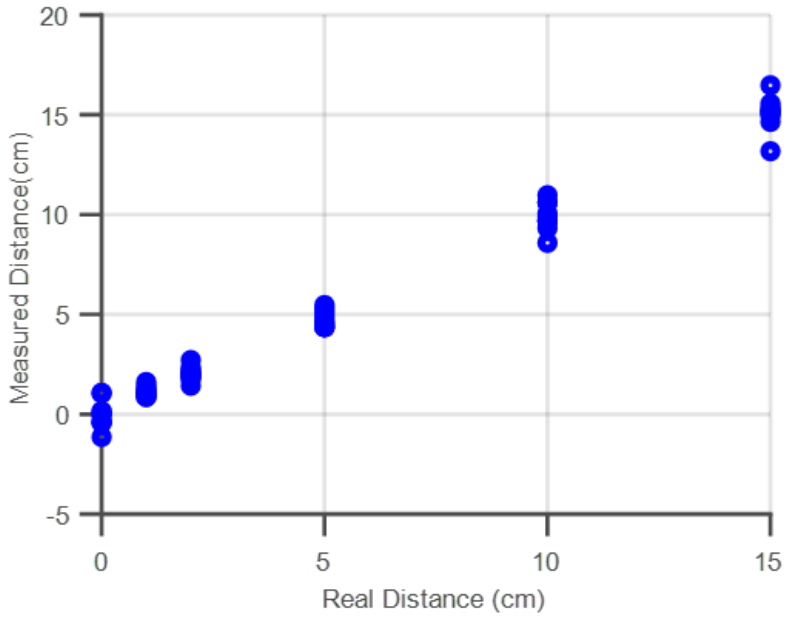

(a)

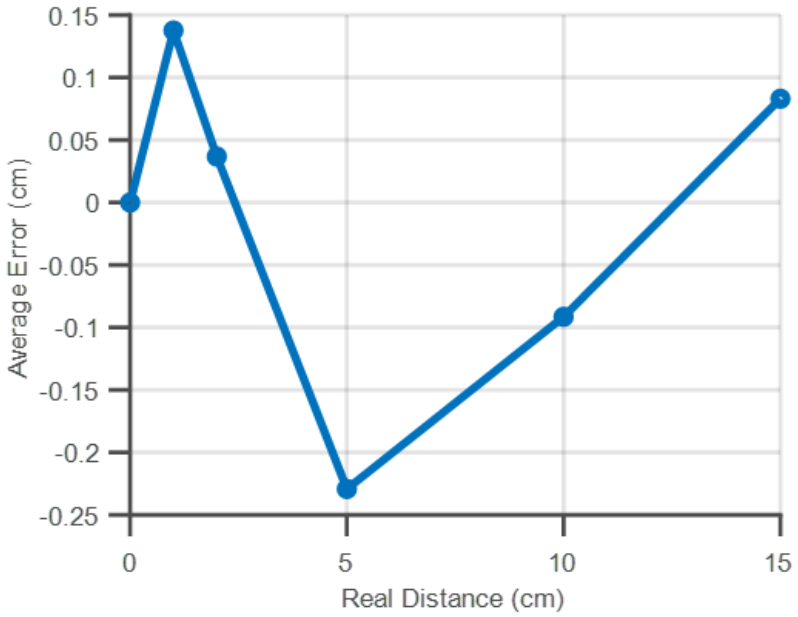

(b)

Figure 4.9: Spectrum averaging method performance: (a) Measured vs. Real Distance Distribution (b) Error vs. Real Distance

Phase based ranging for mmWave RFID

In tracking and some health monitoring applications, it is important to be able to monitor the displacement of some device even more accurately than the sub-centimeter levels demonstrated in the preceding sections [5]. Operating in the $24\,\mathrm{GHz}$ frequency band ensures that we have a phase response very sensitive to small changes in displacement. From the relationship given by $\theta = \beta l$ it can be computed that a $17\,\mu\mathrm{m}$ change in distance corresponds to about a 1° change in phase. This corresponds to a very high accuracy however it is limited by the 2π ambiguity in the phase of a sinusoidal signal which corresponds to a $\frac{\lambda}{2}$ traversal since it is the round-trip distance between the signal and the target being considered [31]. Despite this limitation, the use of phase in radar ranging and localization for different applications have been reported [32, 33]. For a tracking application however, this point of ambiguity is fairly inconsequential given that the phase of the target can be well monitored over time so ambiguities can be resolved based on a-priori knowledge of it's position. We can refer back to equation 2.7 that shows the construction of the received baseband signal. Since $f_{min} >> f_m od >> f_b$, that equation can be simplified to the following given by equation 4.3. The parameter of interest is R and this quantity is embedded in the total phase of the baseband signal received by the reader which also includes the random modulation phase applied at the tag, ϕ_{mod}. This quantity is unknown and thus prevents the extraction of the phase due solely to the propagation of the signal to the target and back to the reader. However, an advantage of combining modulated backscatter with FMCW principles is the fact that we generate two frequency components as shown in equation 4.3. When the Fourier transform of this real signal is taken, there are a total of four complex exponentials obtained. The terms in the negative frequency spectrum have opposite phases to those in the positive spectrum as can be seen in figure 4.10. It is then seen that by taking the sum of the phases of the two highlighted complex exponentials, the modulation phase can be de-embedded and we are then left with $4kR$ as the resultant phase so that changes

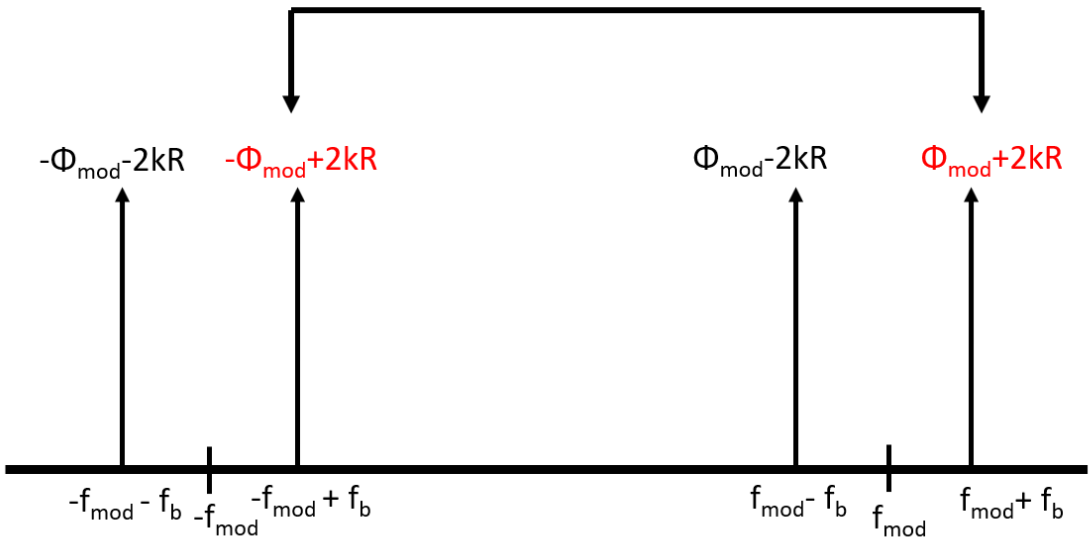

Figure 4.10: Modulation phase de-embedding

in the range of the target, R can be mapped directly to a change in phase.

$$S_b = \frac{1}{2}cos(2\pi((f_{mod}+f_b)t+\phi_{mod}+2kR)+\frac{1}{2}cos(2\pi((f_{mod}-f_b)t+\phi_{mod}-2kR) \quad (4.3)$$

The performance of this prescribed method is done experimentally. A tag set on a track is displaced in front of the reader in steps of $1, 2, 3, 4$ and $5\,\mathrm{mm}$ and the resultant phase is monitored. A total of 10 measurements are taken at each step and the results of this are summarized in figures 4.11a and 4.11b. The plots show that the relative distance measured shows good agreement with the true distance. The maximum error in the determined distance is kept below $0.2\,\mathrm{mm}$.

Given the maximum error achieved in the previous set of measurements, it stands to reason that this method and the developed device could potentially yield accuracy in the sub-mm range. This is tested in a similar manner by setting the tag in front of the reader and moving it in steps of $0.2, 0.4, 0.8$ and $0.8\,\mathrm{mm}$. The results are shown in figures 4.12a

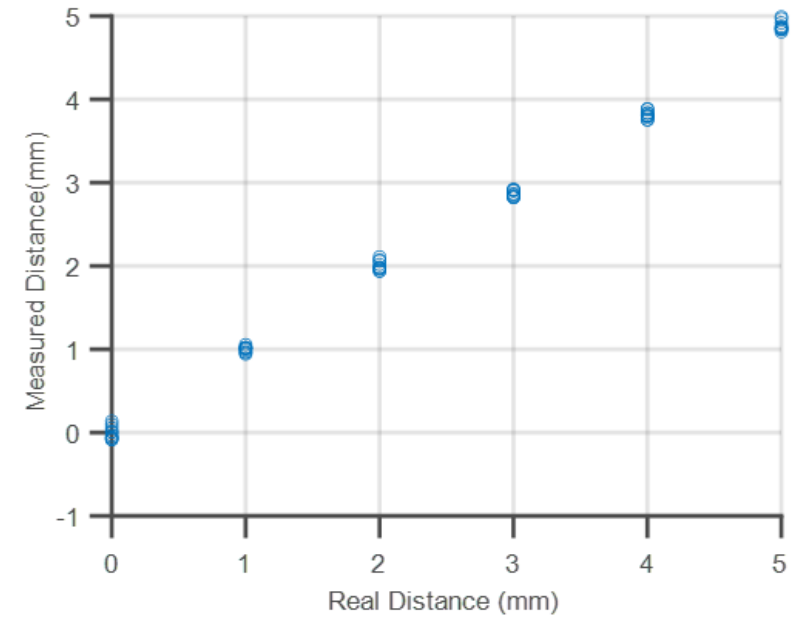

(a)

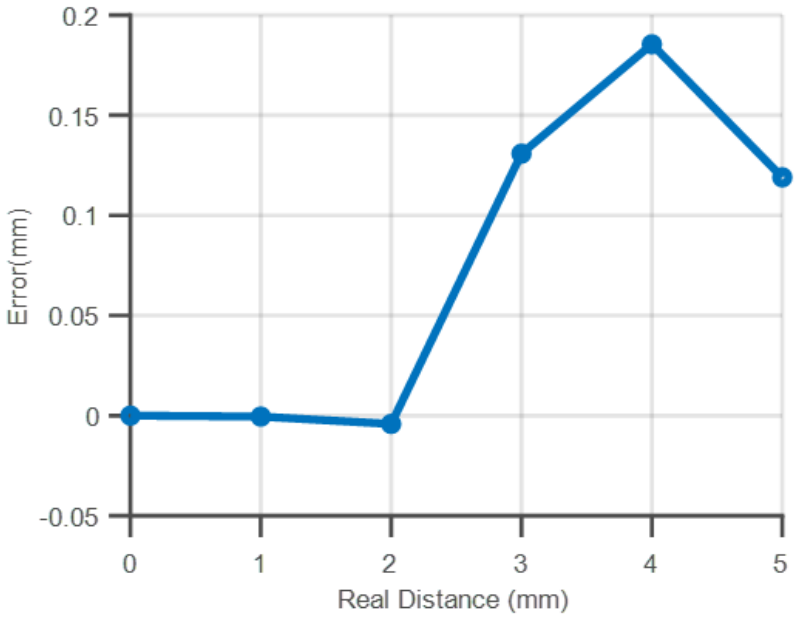

(b)

Figure 4.11: Phase based ranging: (a) Measured vs. Real Distance Distribution (b) Error vs. Real Distance

and 4.12b. Similar to the previous experiment, we are able to see good agreement in the measured and real distances and the maximum error obtained is again less than $0.2\,\mathrm{mm}$.

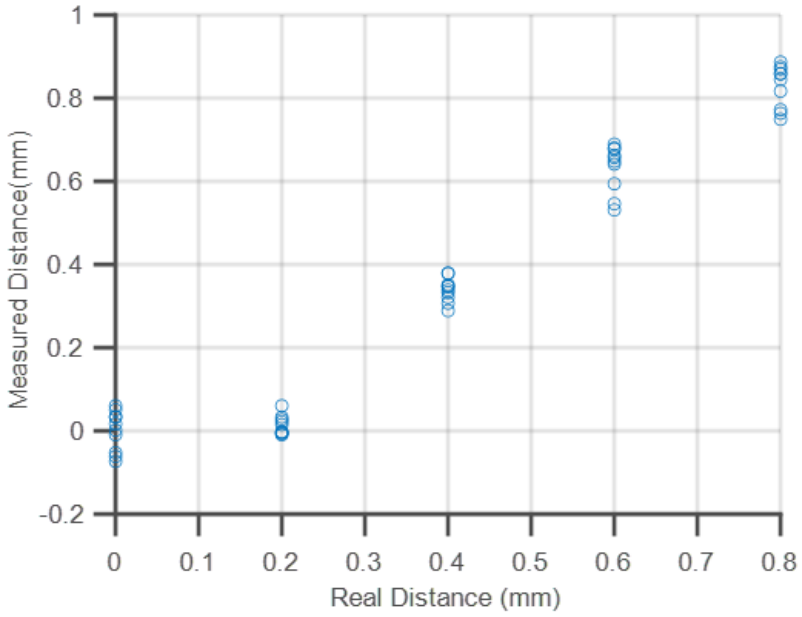

(a)

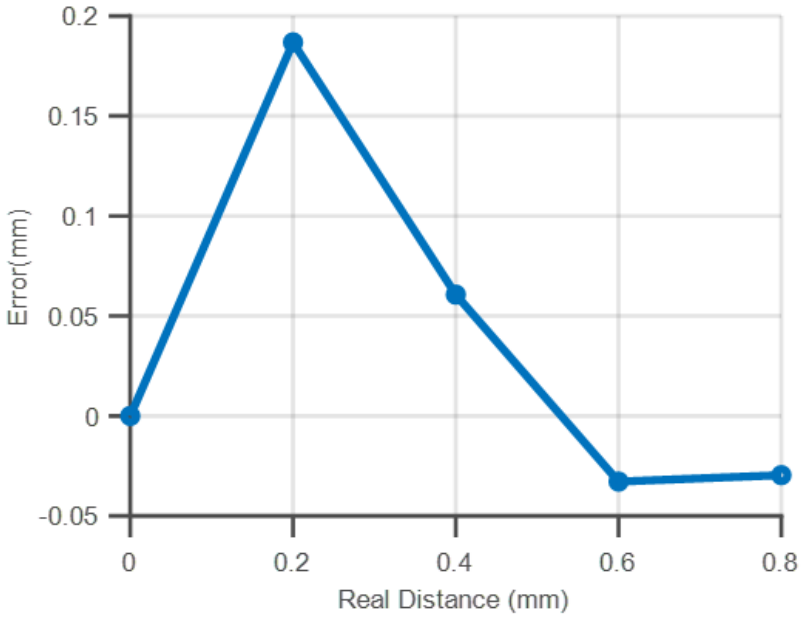

(b)

Figure 4.12: Phase based ranging (sub-mm): (a) Measured vs. Real Distance Distribution (b) Error vs. Real Distance

4.4 Angle of Arrival

After the target modulation frequency and range have been determined, the next piece of information necessary in order to get a full spatial picture of the bakscattering target is the angle in azimuth of the target relative to the interrogating system. This is achieved by spatially sampling the received signal at the reader so that the angle of arrival is obtained as a function of the difference in phase between the signal received at each receiving antenna as described in detail in chapter 2. The spatial FFT behaves just like the well known sum beam-former from array signal processing concepts, it shows a coarse peak at the angle where the target is located. The width of this peak is dependent on the number of receiving antennas such that increased resolution is possible as the number of receiving channels increase.

There is an important pre-processing step needed before the angle of arrival can be reliably extracted. Due to the high clutter/multi-path environment and inconsistencies in connecting cables such as small variations in lengths/bends which would inadvertently affect the phase measurement, it is important to take a calibration measurement at a known angle. This only needs to be done once and can be used repeatedly. A tag is placed in front of the reader as close to bore-sight as possible and a measurement of it's response is captured and used for calibration. The process for extracting the angle of arrival is relatively simple, an FFT is first applied on the sampled baseband data from each of the receiving channels. Once the tag is identified, the local maximum in it's response is taken for each of the channels. It is important for only one of the side-bands to be used in determining the local maximum resulting in one sample taken from each channel measurement. The calibration taken is then applied to these samples to de-embed the effects of the connecting cables and any static environmental effects. After this a zero-padded FFT across the local maxima is taken to reveal the angular spectrum. The result of this process is summarized in figures 4.13a and 4.13b for a series of 10 measurements with the tag oriented at 0° and

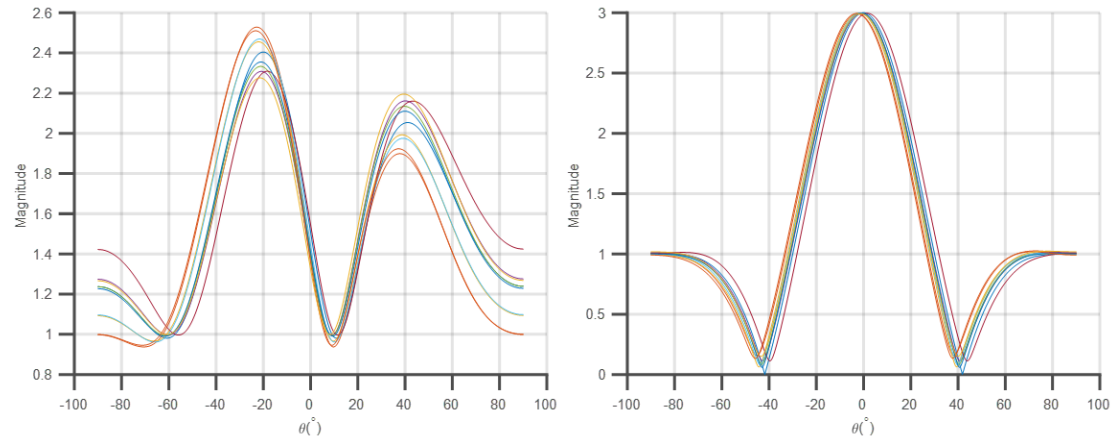

(a)

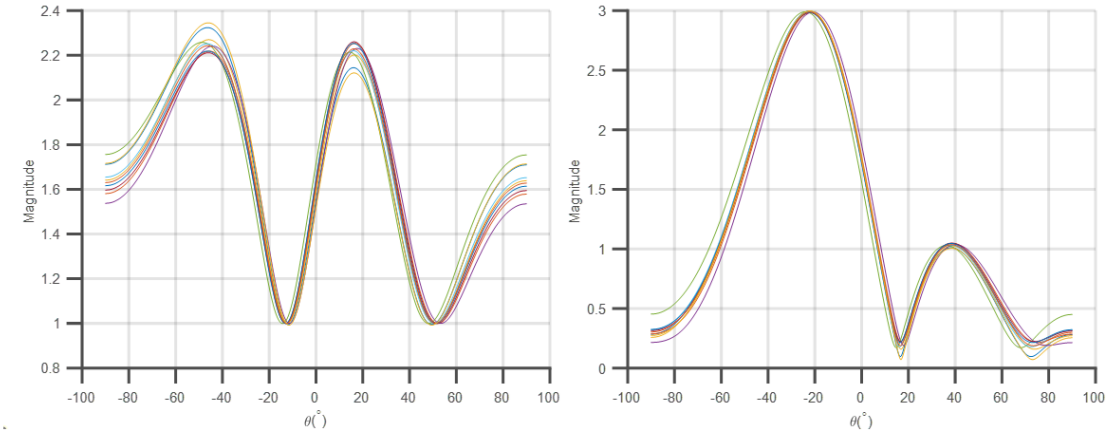

(b)

Figure 4.13: Angle of Arrival Calibration: (a) Before and after calibration at $0\,^\circ$ (b) Error vs. Before and after calibration at $-20\,^\circ$

$-20\,^\circ$ relative to the reader. It is clear from these results that without a proper initial calibration, the system is not able to resolve the correct angle of arrival in either case. We also get a view into the achievable accuracy in angle of arrival measurements with this system.

The accuracy of the angular measurement is then characterized experimentally. The tag was moved between $-40\,^\circ$ and $40\,^\circ$ in steps of $10\,^\circ$ with 10 measurements taken at each step. The same process as described above was applied to extract the angular information. The results of this are summarized in figures 4.14a and 4.14b. A good agreement is shown between the measured angle and the true angle in the measurements conducted and shown

on figure 4.14a. Good error performance is shown in figure 4.14b, it is shown that the error degrades near the edge of the measurement reaching up to $10\,^\circ$ of average error at an angle of $-40\,^\circ$. This occurs as a result of the inverse sine relationship between the phase and the angle of arrival because as the inverse sine approaches ± 1 or the angle of arrival approaches $\pm 90\,^\circ$ the slope of the function increases very quickly so the error can become quite large. This effect can be overcome by extension to MIMO systems having multiple transmitting and receiving antenna to improve the resolution of the angle of arrival estimation process as described here.

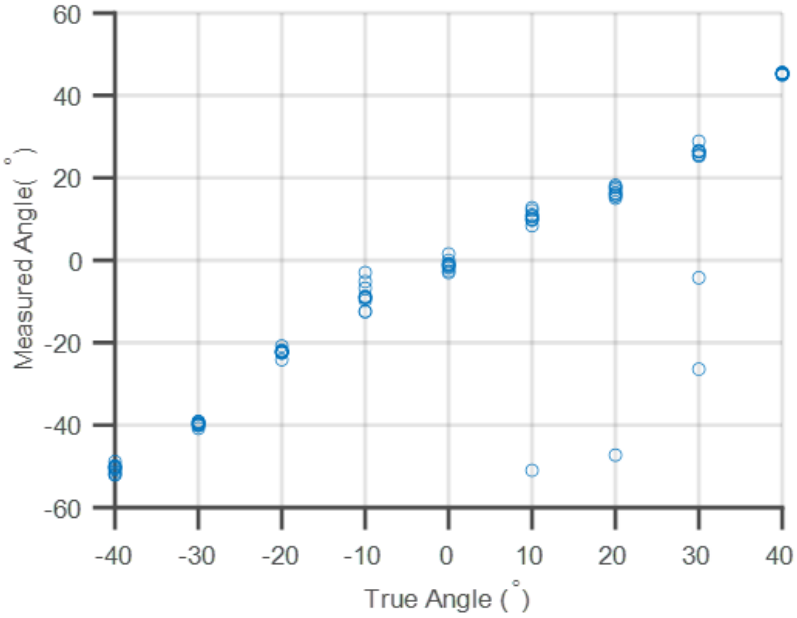

(a)

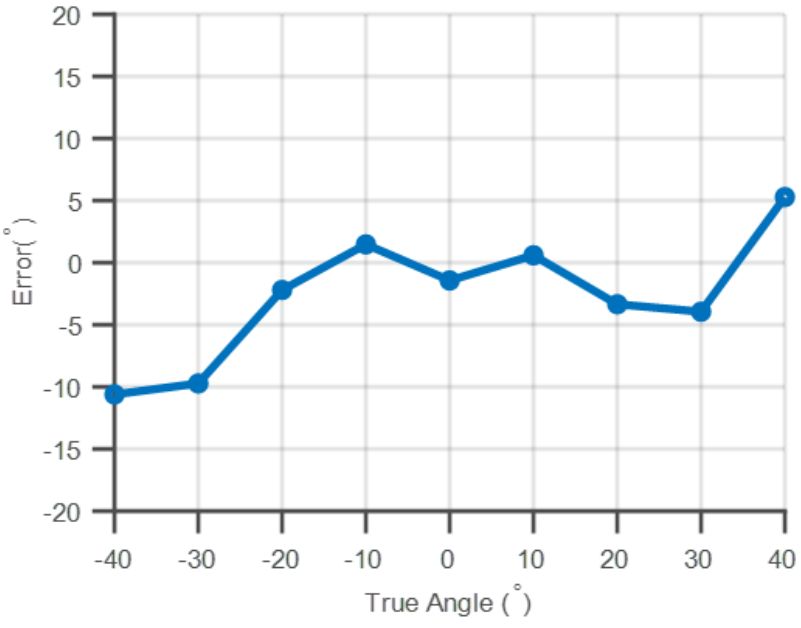

(b)

Figure 4.14: Angle of Arrival: (a) Measured vs. True Angle Distribution (b) Error vs. True Angle

CHAPTER 5
CONCLUSION

In this effort, a first of its kind miniaturized millimeter wave RFID tag capable of unique identification and spatial localization was presented alongside a suggested topology for a chip antenna based energy harvesting system. The millimeter wave compatibility of the proposed RFID tag makes it suitable for a variety of budding 5G and IoT topologies and architectures that require identification and/or localization. The very low form factor and ultra-low power consumption of the proposed device and makes it useful in a variety of low power sensing and detection applications. It was successfully shown that the developed millimeter wave RFID tag is able to be localized and tracked in space to within $0.2\,\mathrm{cm}$ in range and 5° in angular space making it suitable for a large number of applications. The ranging accuracy is increased by observing the change in phase of the target, accuracy to within $0.2\,\mathrm{mm}$ thus allowing it to be used in fine grain localization and coupled sensing applications.

The work presented here can build upon existing implementations of radar based sensors for human gesture recognition [34, 35, 36] or motion capture by allowing the use of an ultra low power reference tag that gives a higher signal to noise ratio which would ease the signal processing burden by avoiding the use of the computationally expensive algorithms required in the passive radar sensing scenario.

REFERENCES

[1] R Miesen, R Ebelt, F Kirsch, T Schäfer, G Li, H Wang, and M Vossiek, "Where is the tag?" *IEEE Microwave Mag.*, vol. 12, no. 7, S49–S63, Dec. 2011.

[2] M Bouet and A. L. dos Santos, "RFID tags: Positioning principles and localization techniques," in *2008 1st IFIP Wireless Days*, Nov. 2008, pp. 1–5.

[3] Y. Ma, N. Selby, and F. Adib, "Minding the billions: Ultra-wideband localization for deployed RFID tags," in *Proceedings of the 23rd Annual International Conference on Mobile Computing and Networking*, ACM, Oct. 2017, pp. 248–260.

[4] J. Heidrich, D. Brenk, J. Essel, S. Schwarzer, K. Seemann, G. Fischer, and R. Weigel, "The roots, rules, and rise of rfid," *IEEE Microwave Magazine*, vol. 11, no. 3, pp. 78–86, 2010.

[5] T Liu, M Hsu, and Z Tsai, "High ranging accuracy and wide detection range interferometry based on Frequency-Sweeping technique with vital sign sensing function," *IEEE Trans. Microw. Theory Tech.*, vol. 66, no. 9, pp. 4242–4251, Sep. 2018.

[6] A. S. Martínez-Sala, E. Egea-López, F. García-Sánchez, and J. García-Haro, "Tracking of returnable packaging and transport units with active rfid in the grocery supply chain," *Computers in Industry*, vol. 60, no. 3, pp. 161–171, 2009, INTELLIGENT PRODUCTS.

[7] X. Li, Y. Zhang, and M. G. Amin, "Multifrequency-based range estimation of rfid tags," in *2009 IEEE International Conference on RFID*, 2009, pp. 147–154.

[8] V. Lakafosis and M. M. Tentzeris, "From single-to multihop: The status of wireless localization," *IEEE Microwave Magazine*, vol. 10, no. 7, pp. 34–41, 2009.

[9] J. Wang and D. Katabi, "Dude, where's my card?: RFID positioning that works with multipath and non-line of sight," in *Proceedings of the ACM SIGCOMM 2013 Conference on SIGCOMM*, ser. SIGCOMM '13, Hong Kong, China: ACM, 2013, pp. 51–62.

[10] A. Strobel, C. Carlowitz, R. Wolf, F. Ellinger, and M. Vossiek, "A millimeter-wave low-power active backscatter tag for fmcw radar systems," *IEEE Transactions on Microwave Theory and Techniques*, vol. 61, no. 5, pp. 1964–1972, 2013.

[11] M. Vossiek and P. Gulden, "The switched injection-locked oscillator: A novel versatile concept for wireless transponder and localization systems," *IEEE Transactions on Microwave Theory and Techniques*, vol. 56, no. 4, pp. 859–866, 2008.

[12] K Wang, J Gu, F Ren, and K Wu, "A multitarget active backscattering 2-D positioning system with superresolution time series Post-Processing technique," *IEEE Trans. Microw. Theory Tech.*, vol. 65, no. 5, pp. 1751–1766, May 2017.

[13] J. G. D. Hester and M. M. Tentzeris, "A mm-wave ultra-long-range energy-autonomous printed RFID-enabled van-atta wireless sensor: At the crossroads of 5G and IoT," in *2017 IEEE MTT-S International Microwave Symposium (IMS)*, Jun. 2017, pp. 1557–1560.

[14] S. J. Thomas, E. Wheeler, J. Teizer, and M. S. Reynolds, "Quadrature amplitude modulated backscatter in passive and semipassive uhf rfid systems," *IEEE Transactions on Microwave Theory and Techniques*, vol. 60, no. 4, pp. 1175–1182, 2012.

[15] P. Nikitin and K. Rao, "Theory and measurement of backscattering from rfid tags," *IEEE Antennas and Propagation Magazine*, vol. 48, no. 6, pp. 212–218, 2006.

[16] F Guidi, N Decarli, D Dardari, F Mani, and R D'Errico, "Passive Millimeter-Wave RFID using backscattered signals," in *2016 IEEE Globecom Workshops (GC Wkshps)*, Dec. 2016, pp. 1–6.

[17] H. Ding, M. Xi, Z. Li, and J. Zhao, "Device-Free mobile target tracking using passive tags," *Int. J. Distrib. Sens. Netw.*, vol. 11, no. 11, p. 870 204, Nov. 2015.

[18] J. Lorenzo, A. Lazaro, R. Villarino, and D. Girbau, "Active backscatter transponder for fmcw radar applications," *IEEE Antennas and Wireless Propagation Letters*, vol. 14, pp. 1610–1613, 2015.

[19] W. Scheiblhofer, R. Feger, A. Haderer, S. Scheiblhofer, and A. Stelzer, "Simultaneous localization and data-interrogation using a 24-ghz modulated-reflector fmcw radar system," in *2017 IEEE MTT-S International Microwave Symposium (IMS)*, 2017, pp. 67–70.

[20] T Kiuru, P Pursula, J Rajamäki, and T Vähä-Heikkilä, "A 60-GHz semipassive MMID transponder for backscattering communications," in *2013 IEEE MTT-S International Microwave Symposium Digest (MTT)*, Jun. 2013, pp. 1–3.

[21] J.-F. Gu, K. Wang, and K. Wu, "System architecture and signal processing for frequency-modulated continuous-wave radar using active backscatter tags," *IEEE Transactions on Signal Processing*, vol. 66, no. 9, pp. 2258–2272, 2018.

[22] S. Suleymanov, "Design and implementation of an FMCW radar signal processing module for automotive applications," Master's thesis, University of Twente, 2016.

[23] J. D. Griffin and G. D. Durgin, "Complete link budgets for Backscatter-Radio and RFID systems," *ISSN*, vol. 1045, p. 9243, 2009.

[24] S. Mercier, D. Roque, and S. Bidon, "Successive self-interference cancellation in a low-complexity wcp-ofdm radar receiver," in *2018 52nd Asilomar Conference on Signals, Systems, and Computers*, 2018, pp. 712–716.

[25] J. G. D. Hester and M. M. Tentzeris, "Inkjet-printed flexible mm-wave Van-Atta reflectarrays: A solution for ultralong-range dense multitag and multisensing chipless RFID implementations for IoT smart . . .," *IEEE Trans. Microw. Theory Tech.*, 2016.

[26] J. A. Vitaz, A. M. Buerkle, M. Sallin, and K. Sarabandi, "Enhanced detection of on-metal retro-reflective tags in cluttered environments using a polarimetric technique," *IEEE Transactions on Antennas and Propagation*, vol. 60, no. 8, pp. 3727–3735, 2012.

[27] *20 / 24 ghz super low noise fet in hollow plastic pkg*, CE3520K3, California Eastern Laboratories, 2019.

[28] *915 mhz ceramic chip antenna*, ACAG1204-915-T, ABRACON, 2018.

[29] M. D. Macleod, "Fast nearly ML estimation of the parameters of real or complex single tones or resolved multiple tones," *IEEE Trans. Signal Process.*, vol. 46, no. 1, pp. 141–148, Jan. 1998.

[30] A. O. Adeyeye, J Hester, and M. M. Tentzeris, "Miniaturized millimeter wave RFID tag for spatial identification and localization in internet of things applications," in *2019 49th European Microwave Conference (EuMC)*, Oct. 2019, pp. 105–108.

[31] S Scherr, S Ayhan, M Pauli, and T Zwick, "Accuracy limits of a k-band FMCW radar with phase evaluation," in *2012 9th European Radar Conference*, Oct. 2012, pp. 246–249.

[32] J. Yan, G. Zhang, H. Hong, H. Chu, C. Li, and X. Zhu, "Phase-based human target 2-d identification with a mobile fmcw radar platform," *IEEE Transactions on Microwave Theory and Techniques*, vol. 67, no. 12, pp. 5348–5359, 2019.

[33] J. Park, D.-H. Jung, K.-B. Bae, and S.-O. Park, "Range-doppler map improvement in fmcw radar for small moving drone detection using the stationary point concentration technique," *IEEE Transactions on Microwave Theory and Techniques*, vol. 68, no. 5, pp. 1858–1871, 2020.

[34] H.-S. Yeo, R. Minami, K. Rodriguez, G. Shaker, and A. Quigley, "Exploring tangible interactions with radar sensing," *Proceedings of the ACM on Interactive, Mobile, Wearable and Ubiquitous Technologies*, vol. 2, no. 4, p. 200, Dec. 2018.

[35] J. Lien, N. Gillian, M. E. Karagozler, P. Amihood, C. Schwesig, E. Olson, H. Raja, and I. Poupyrev, "Soli: Ubiquitous gesture sensing with millimeter wave radar," *ACM Transactions on Graphics (TOG)*, vol. 35, no. 4, pp. 1–19, 2016.

[36] C. Gu, J. Wang, and J. Lien, "Motion sensing using radar: Gesture interaction and beyond," *IEEE Microwave Magazine*, vol. 20, no. 8, pp. 44–57, 2019.